

Exploring dark matter, neutrino mass and $R_{K^{(*)},\phi}$ anomalies in $L_\mu - L_\tau$ model

Shivaramakrishna Singirala^{a,*}, Suchismita Sahoo^{b,†} and Rukmani Mohanta^{a,‡}

^a*School of Physics, University of Hyderabad, Hyderabad-500046, India*

^b*Theoretical Physics Division, Physical Research Laboratory, Ahmedabad-380009, India*

Abstract

We investigate Majorana dark matter in a new variant of $U(1)_{L_\mu-L_\tau}$ gauge extension of Standard Model, where the scalar sector is enriched with an inert doublet and a $(\bar{3}, 1, 1/3)$ scalar leptoquark. We compute the WIMP-nucleon cross section in leptoquark portal and the relic density mediated by inert doublet components, leptoquark and the new Z' boson. We constrain the parameter space consistent with Planck limit on relic density, PICO-60 and LUX bounds on spin-dependent direct detection cross section. Furthermore, we constrain the new couplings from the present experimental data on $\text{Br}(\tau \rightarrow \mu\nu_\tau\bar{\nu}_\mu)$, $\text{Br}(B \rightarrow X_s\gamma)$, $\text{Br}(\bar{B}^0 \rightarrow \bar{K}^0\mu^+\mu^-)$, $\text{Br}(B^+ \rightarrow K^+\tau^+\tau^-)$ and $B_s - \bar{B}_s$ mixing, which occur at one-loop level in the presence of Z' and leptoquark. Using the allowed parameter space, we estimate the form factor independent $P'_{4,5}$ observables and the lepton non-universality parameters R_K , R_{K^*} and R_ϕ . We also briefly discuss about the neutrino mass generation at one-loop level and the viable parameter region to explain current neutrino oscillation data.

*Electronic address: krishnas542@gmail.com

†Electronic address: suchismita8792@gmail.com

‡Electronic address: rmsp@uohyd.ernet.in

I. INTRODUCTION

Though the experimental measured values of various physical observables are in excellent agreement with the Standard Model (SM) predictions, there are many open unsolved problems like the matter-antimatter asymmetry, hierarchy problem and the dark matter (DM) content of the universe etc., which make ourselves believe that there is something beyond the SM. In this regard, the study of rare semileptonic B decay processes provide an ideal testing ground to critically test the SM and to look for possible extension of it. Although, so far we have not observed any clear indication of new physics (NP) in the B sector, there are several physical observables associated with flavor changing neutral current (FCNC) $b \rightarrow sl^+l^-$ processes which have $(2 - 4)\sigma$ [1–6] discrepancies. Especially, the observation of 3σ anomaly in the P'_5 angular observables [4] and the decay rate [5] of $B^0 \rightarrow K^{*0}\mu^+\mu^-$ processes have attracted a lot of attention in recent times. The decay rate of $B_s \rightarrow \phi\mu^+\mu^-$ has also 3σ deviation compared to its SM prediction [3]. Furthermore, the LHCb Collaboration has observed the violation of lepton universality in $B^+ \rightarrow K^+l^+l^-$ process in the low $q^2 \in [1, 6]$ GeV² region [2]

$$R_K^{\text{Expt}} = \frac{\text{Br}(B^+ \rightarrow K^+\mu^+\mu^-)}{\text{Br}(B^+ \rightarrow K^+e^+e^-)} = 0.745_{-0.074}^{+0.090} \pm 0.036, \quad (1)$$

which has a 2.6σ deviation from the corresponding SM result [7]

$$R_K^{\text{SM}} = 1.0003 \pm 0.0001. \quad (2)$$

In addition, an analogous lepton non-universality (LNU) parameter (R_{K^*}) has also been observed in $B^0 \rightarrow K^{*0}l^+l^-$ processes [1]

$$\begin{aligned} R_{K^*}^{\text{Expt}} &= \frac{\text{Br}(B^0 \rightarrow K^{*0}\mu^+\mu^-)}{\text{Br}(B^0 \rightarrow K^{*0}e^+e^-)} = 0.66_{-0.07}^{+0.11} \pm 0.03, & q^2 \in [0.045, 1.1] \text{ GeV}^2, \\ &= 0.69_{-0.07}^{+0.11} \pm 0.05, & q^2 \in [1.1, 6] \text{ GeV}^2, \end{aligned} \quad (3)$$

which correspond to the deviation of 2.2σ and 2.4σ from their SM predictions [8]

$$R_{K^*}^{\text{SM}}|_{q^2 \in [0.045, 1.1] \text{ GeV}^2} = 0.92 \pm 0.02, \quad R_{K^*}^{\text{SM}}|_{q^2 \in [1.1, 6] \text{ GeV}^2} = 1.00 \pm 0.01. \quad (4)$$

To resolve the above $b \rightarrow sll$ anomalies, we extend the SM gauge group $SU(3)_C \times SU(2)_L \times U(1)_Y$ with a local $U(1)_{L_\mu - L_\tau}$ symmetry. The anomaly free $L_\mu - L_\tau$ gauge extensions [9, 10] are captivating with minimal new particles and parameters, rich in phenomenological

perspective. The model is quite simple in structure, suitable to study the phenomenology of DM, neutrino and also the flavor anomalies [11–15]. It is well explored in dark matter context in literature [12–15], in the gauge and scalar portals. In the literature [16–19], the DM, neutrino and flavor phenomenology are also investigated in several $U(1)$ extended models. The approach of adding color triplet particles to shed light on the flavor sector thereby connecting with dark sector is interesting. Leptoquarks (LQ) are not only advantageous in addressing the flavor anomalies, but also act as a mediator between the visible and dark sector. Few works were already done with this motivation [20–23].

Leptoquarks are hypothetical color triplet gauge particles, with either spin-0 (scalar) or spin-1 (vector), which connect the quark and lepton sectors and thus, carry both baryon and lepton numbers simultaneously. They can arise from various extended standard model scenarios [24–35], which treat quarks and leptons on equal footing, such as the grand unified theories (GUTs) [24–27], color $SU(4)$ Pati-Salam model [28–32], extended technicolor model [33, 34] and the composite models of quark and lepton [35]. In this article, we study a new version of $U(1)_{L_\mu-L_\tau}$ gauge extension of SM with a $(\bar{3}, 1, 1/3)$ scalar LQ (SLQ) and an inert doublet, to study the phenomenology of dark matter, neutrino mass generation and compute the flavor observables on a single platform. The SLQ mediates the annihilation channels contributing to relic density and also plays a crucial role in direct searches as well, providing a spin-dependent WIMP-nucleon cross section which is quite sensitive to the recent and ongoing direct detection experiments such as PICO-60 and LUX. The Z' gauge boson of extended $U(1)$ symmetry and the SLQ also play an important role in settling the known issues of flavor sector. In this regard, we would like to investigate whether the observed anomalies in the rare leptonic/semileptonic decay processes mediated by $b \rightarrow sl^+l^-$ transitions, can be explained in the present framework. We analyze the implications of the model on both the DM and flavor sectors, in particular on $B \rightarrow Vl^+l^-$ ($V = K^*, \phi$) decay modes. In literature [36–59], there were many attempts being made to explain the observed anomalies of rare B decays in the scalar leptoquark model.

The paper is structured as follows. We describe the particle content, relevant Lagrangian and interaction terms, pattern of symmetry breaking in section-II. We derive the mass eigenstates of the new fermions and the scalar spectrum in section-III. We then provide a detailed study of DM phenomenology in prospects of relic density and direct detection observables in section-IV. The mechanism of generating light neutrino mass at one-loop level,

consistent with the current oscillation data is illustrated in section V. Section-VI contains the additional constraint on the new parameters obtained from the existing anomalies of the flavor sector, like $\text{Br}(\tau \rightarrow \mu\nu_\tau\bar{\nu}_\mu)$, $\text{Br}(B \rightarrow X_s\gamma)$, $\text{Br}(\bar{B}^0 \rightarrow \bar{K}^0\mu^+\mu^-)$, $\text{Br}(B^+ \rightarrow K^+\tau\tau)$ and $B_s - \bar{B}_s$ mixing. We then investigate the impact of additional $U(1)_{L_\mu-L_\tau}$ gauge symmetry on the $R_{K^{(*)}}$, R_ϕ LNU parameters and optimized $P'_{4,5}$ observables in section-VII. We summarize our findings in Section-VIII.

II. NEW $L_\mu - L_\tau$ MODEL WITH A SCALAR LEPTOQUARK

We study the well known anomaly free $U(1)_{L_\mu-L_\tau}$ extension of SM containing three additional neutral fermions N_e, N_μ, N_τ , with $L_\mu - L_\tau$ charges 0, 1 and -1 respectively. A scalar singlet ϕ_2 , charged $+2$ under the new $U(1)$ is added to spontaneously break the local $U(1)_{L_\mu-L_\tau}$ gauge symmetry. We also introduce an inert doublet η and a scalar leptoquark $S_1(\bar{3}, 1, 1/3)$ with $L_\mu - L_\tau$ charges 0 and -1 to the scalar content of the model. We impose an additional Z_2 symmetry under which all the new fermions, η and the leptoquark are odd and rest are even. The particle content and their corresponding charges are displayed in Table. I.

The Lagrangian of the present model can be written as

$$\begin{aligned}
\mathcal{L} = & \mathcal{L}_{\text{SM}} - \frac{1}{4}Z'_{\mu\nu}Z'^{\mu\nu} - g_{\mu\tau}\bar{\mu}_L\gamma^\mu\mu_L Z'_\mu - g_{\mu\tau}\bar{\mu}_R\gamma^\mu\mu_R Z'_\mu + g_{\mu\tau}\bar{\tau}_L\gamma^\mu\tau_L Z'_\mu + g_{\mu\tau}\bar{\tau}_R\gamma^\mu\tau_R Z'_\mu \\
& + \bar{N}_e i\not{\partial} N_e + \bar{N}_\mu (i\not{\partial} - g_{\mu\tau} Z'_\mu \gamma^\mu) N_\mu + \bar{N}_\tau (i\not{\partial} + g_{\mu\tau} Z'_\mu \gamma^\mu) N_\tau - \frac{f_\mu}{2} (\bar{N}_\mu^c N_\mu \phi_2^\dagger + \text{h.c.}) \\
& - \frac{f_\tau}{2} (\bar{N}_\tau^c N_\tau \phi_2 + \text{h.c.}) - \frac{1}{2} M_{ee} \bar{N}_e^c N_e - \frac{1}{2} M_{\mu\tau} (\bar{N}_\mu^c N_\tau + \bar{N}_\tau^c N_\mu) - \sum_{q=d,s,b} (y_{qR} \bar{d}_{qR}^c S_1 N_\mu + \text{h.c.}) \\
& - \sum_{l=e,\mu,\tau} (Y_{\beta l} (\bar{\ell}_L)_\beta \tilde{\eta} N_{lR} + \text{h.c.}) + \left| \left(i\partial_\mu - \frac{g}{2} \boldsymbol{\tau}^a \cdot \mathbf{W}_\mu^a - \frac{g'}{2} B_\mu \right) \eta \right|^2 + \left| \left(i\partial_\mu - \frac{g'}{3} B_\mu + g_{\mu\tau} Z'_\mu \right) S_1 \right|^2 \\
& + \left| (i\partial_\mu - 2g_{\mu\tau} Z'_\mu) \phi_2 \right|^2 - V(H, \eta, \phi_2, S_1), \tag{5}
\end{aligned}$$

where the scalar potential V is

$$\begin{aligned}
V(H, \eta, \phi_2, S_1) = & \mu_H^2 H^\dagger H + \lambda_H (H^\dagger H)^2 + \mu_\eta (\eta^\dagger \eta) + \lambda_{H\eta} (H^\dagger H) (\eta^\dagger \eta) + \lambda_\eta (\eta^\dagger \eta)^2 + \lambda'_{H\eta} (H^\dagger \eta) (\eta^\dagger H) \\
& + \frac{\lambda''_{H\eta}}{2} [(H^\dagger \eta)^2 + \text{h.c.}] + \mu_2^2 (\phi_2^\dagger \phi_2) + \lambda_2 (\phi_2^\dagger \phi_2)^2 + \mu_S^2 (S_1^\dagger S_1) + \lambda_S (S_1^\dagger S_1)^2 \\
& + \left[\lambda_{H2} (\phi_2^\dagger \phi_2) + \lambda_{HS} (S_1^\dagger S_1) \right] (H^\dagger H) + \lambda_{S2} (\phi_2^\dagger \phi_2) (S_1^\dagger S_1) + \lambda_{\eta 2} (\phi_2^\dagger \phi_2) (\eta^\dagger \eta) \\
& + \lambda_{S\eta} (S_1^\dagger S_1) (\eta^\dagger \eta). \tag{6}
\end{aligned}$$

	Field	$SU(3)_C \times SU(2)_L \times U(1)_Y$	$U(1)_{L_\mu-L_\tau}$	Z_2
Fermions	$Q_L \equiv (u, d)_L^T$	$(\mathbf{3}, \mathbf{2}, 1/6)$	0	+
	u_R	$(\mathbf{3}, \mathbf{1}, 2/3)$	0	+
	d_R	$(\mathbf{3}, \mathbf{1}, -1/3)$	0	+
	$e_L \equiv (\nu_e, e)_L^T$	$(\mathbf{1}, \mathbf{2}, -1/2)$	0	+
	e_R	$(\mathbf{1}, \mathbf{1}, -1)$	0	+
	$\mu_L \equiv (\nu_\mu, \mu)_L^T$	$(\mathbf{1}, \mathbf{2}, -1/2)$	1	+
	μ_R	$(\mathbf{1}, \mathbf{1}, -1)$	1	+
	$\tau_L \equiv (\nu_\tau, \tau)_L^T$	$(\mathbf{1}, \mathbf{2}, -1/2)$	-1	+
	τ_R	$(\mathbf{1}, \mathbf{1}, -1)$	-1	+
	N_e	$(\mathbf{1}, \mathbf{1}, 0)$	0	-
	N_μ	$(\mathbf{1}, \mathbf{1}, 0)$	1	-
	N_τ	$(\mathbf{1}, \mathbf{1}, 0)$	-1	-
Scalars	H	$(\mathbf{1}, \mathbf{2}, 1/2)$	0	+
	η	$(\mathbf{1}, \mathbf{2}, 1/2)$	0	-
	ϕ_2	$(\mathbf{1}, \mathbf{1}, 0)$	2	+
	S_1	$(\bar{\mathbf{3}}, \mathbf{1}, 1/3)$	-1	-

TABLE I: Fields and their charges of the proposed $U(1)_{L_\mu-L_\tau}$ model.

The gauge symmetry $SU(2)_L \times U(1)_Y \times U(1)_{L_\mu-L_\tau}$ is spontaneously broken to $SU(2)_L \times U(1)_Y$ by assigning a VEV v_2 to the complex singlet ϕ_2 . Then the SM Higgs doublet breaks the SM gauge group to low energy theory by obtaining a VEV v . The new neutral gauge boson Z' associated with the $U(1)$ extension absorbs the massless pseudoscalar in ϕ_2 to become massive. The neutral components of the fields H and ϕ_2 can be written in terms of real scalars and pseudoscalars as

$$\begin{aligned}
H^0 &= \frac{1}{\sqrt{2}}(v + h) + \frac{i}{\sqrt{2}}A^0, \\
\phi_2 &= \frac{1}{\sqrt{2}}(v_2 + h_2) + \frac{i}{\sqrt{2}}A_2.
\end{aligned} \tag{7}$$

The inert doublet is denoted by $\eta = \begin{pmatrix} \eta^+ \\ \eta^0 \end{pmatrix}$, with $\eta^0 = \frac{\eta_e + i\eta_o}{\sqrt{2}}$. The masses of its charged

and neural components are given by

$$\begin{aligned}
M_{\eta^+}^2 &= \mu_\eta^2 + \frac{\lambda_{H\eta}}{2}v^2 + \frac{\lambda_{\eta 2}}{2}v_2^2, \\
M_{\eta_e}^2 &= \mu_\eta^2 + \frac{\lambda_{\eta 2}}{2}v_2^2 + (\lambda_{H\eta} + \lambda'_{H\eta} + \lambda''_{H\eta})\frac{v^2}{2}, \\
M_{\eta_o}^2 &= \mu_\eta^2 + \frac{\lambda_{\eta 2}}{2}v_2^2 + (\lambda_{H\eta} + \lambda'_{H\eta} - \lambda''_{H\eta})\frac{v^2}{2}.
\end{aligned} \tag{8}$$

The masses obtained by the colored scalar and the gauge boson Z' are

$$\begin{aligned}
M_{S_1}^2 &= 2\mu_S^2 + \lambda_{HS}v^2 + \lambda_{S2}v_2^2, \\
M_{Z'} &= 2v_2g_{\mu\tau}.
\end{aligned} \tag{9}$$

In the whole discussion of the results, we consider the benchmark values for the masses of the scalar spectrum as $(M_{S_1}, M_{\eta^+}, M_{\eta_{e,o}}) = (1.2, 2, 1.5)$ TeV.

III. MIXING IN THE FERMION AND SCALAR SECTOR

The fermion and scalar mass matrices take the form

$$M_N = \begin{pmatrix} \frac{1}{\sqrt{2}}f_\mu v_2 & M_{\mu\tau} \\ M_{\mu\tau} & \frac{1}{\sqrt{2}}f_\tau v_2 \end{pmatrix}, \quad M_S = \begin{pmatrix} 2\lambda_H v^2 & \lambda_{H2} v v_2 \\ \lambda_{H2} v v_2 & 2\lambda_2 v_2^2 \end{pmatrix}. \tag{10}$$

One can diagonalize the above mass matrices by $U_{\alpha(\zeta)}^T M_{N(S)} U_{\alpha(\zeta)} = \text{diag} [M_{N_-(H_1)}, M_{N_+(H_2)}]$, where

$$U_\theta = \begin{pmatrix} \cos \theta & \sin \theta \\ -\sin \theta & \cos \theta \end{pmatrix}, \tag{11}$$

with $\zeta = \frac{1}{2} \tan^{-1} \left(\frac{\lambda_{H2} v v_2}{\lambda_2 v_2^2 - \lambda_H v^2} \right)$ and $\alpha = \frac{1}{2} \tan^{-1} \left(\frac{2M_{\mu\tau}}{(f_\tau - f_\mu)(v_2/\sqrt{2})} \right)$.

We denote the scalar mass eigenstates as H_1 and H_2 , with H_1 is assumed to be observed Higgs at LHC with $M_{H_1} = 125.09$ GeV and $v = 246$ GeV. The mixing parameter ζ is taken minimal to stay with LHC limits on Higgs decay width. We indicate N_- and N_+ to be the fermion mass eigenstates, with the lightest one (N_-) as the probable dark matter candidate in the present work.

IV. DARK MATTER PHENOMENOLOGY

A. Relic abundance

The model allows the dark matter (N_-) to have gauge and scalar mediated annihilation channels. The possible contributing diagrams are provided in Fig. 1 which are mediated by $(H_1, H_2, \eta^+, \eta^0, S_1, Z')$. Majorana DM in $H_{1,2}$ portal (upper row in Fig. 1) has already been well explored in literature [60, 61]. Here, we focus on (Z', S_1, η) -mediated channels (middle and bottom rows in Fig. 1) contributing to DM observables, which we later make connection with radiative neutrino mass as well as flavor observables. The relic abundance

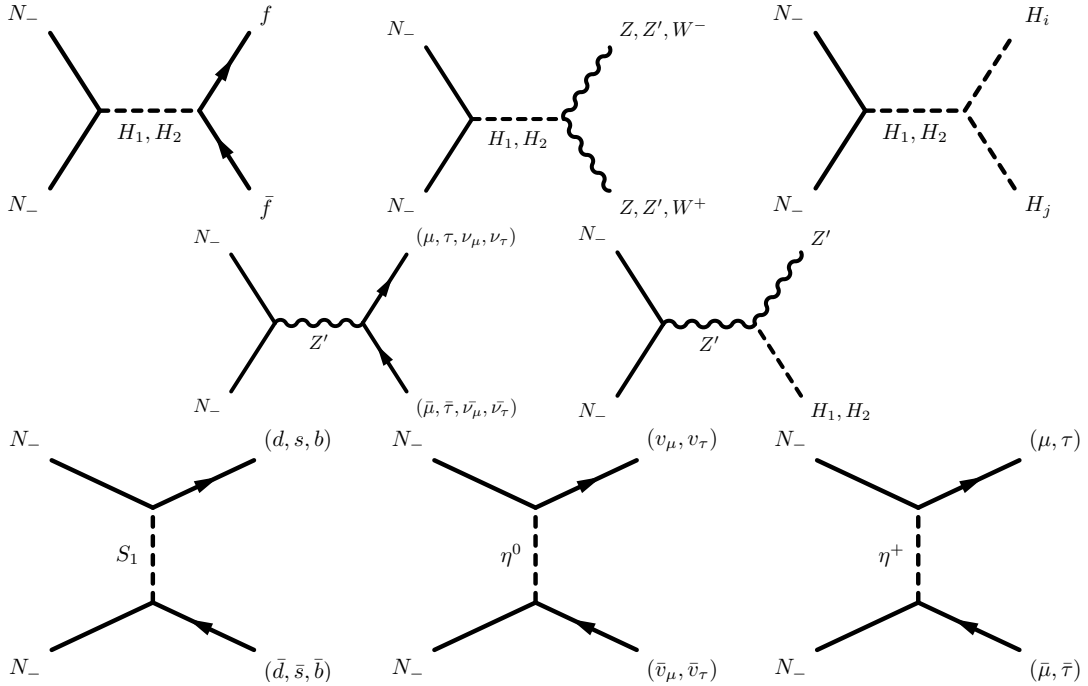


FIG. 1: Feynman diagrams contributing to relic density.

of dark matter is computed by

$$\Omega h^2 = \frac{1.07 \times 10^9 \text{ GeV}^{-1}}{M_{\text{Pl}} g_*^{1/2}} \frac{1}{J(x_f)}. \quad (12)$$

Here the Planck mass, $M_{\text{Pl}} = 1.22 \times 10^{19} \text{ GeV}$ and $g_* = 106.75$ denotes the total number of effective relativistic degrees of freedom. The function $J(x_f)$ reads as

$$J(x_f) = \int_{x_f}^{\infty} \frac{\langle \sigma v \rangle(x)}{x^2} dx. \quad (13)$$

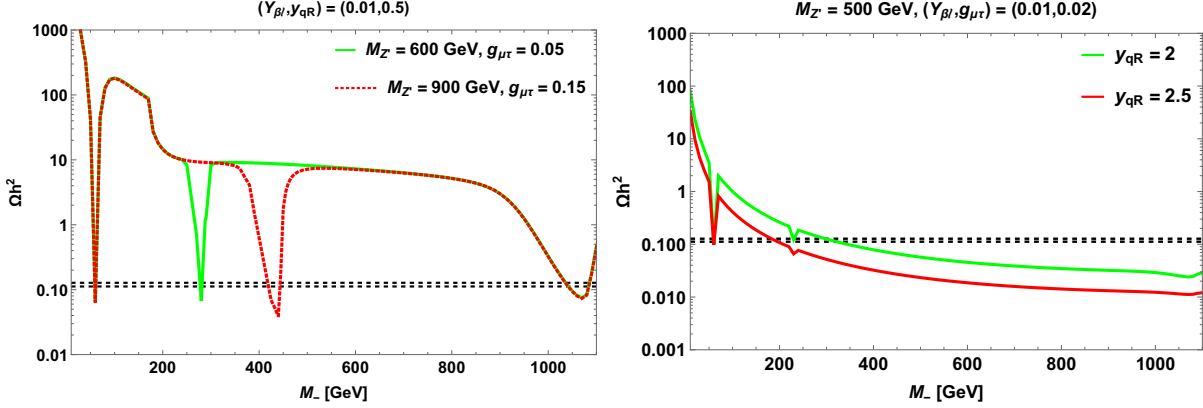


FIG. 2: Behavior of relic density plotted against DM mass with $M_{H_2} = 2.2$ TeV, shown with varying $M_{Z'}$ and $g_{\mu\tau}$ (left panel) and y_{qR} (right panel). Black horizontal dotted lines denote the 3σ range of Planck limit [62].

The thermally averaged annihilation cross section $\langle\sigma v\rangle$ is given by the expression

$$\langle\sigma v\rangle(x) = \frac{x}{8M_-^5 K_2^2(x)} \int_{4M_-^2}^{\infty} \hat{\sigma} \times (s - 4M_-^2) \sqrt{s} K_1\left(\frac{x\sqrt{s}}{M_-}\right) ds, \quad (14)$$

where K_1, K_2 denote the modified Bessel functions, $x = M_-/T$, with T is the temperature and $\hat{\sigma}$ is the dark matter annihilation cross section. The analytical expression for the freeze out parameter x_f is

$$x_f = \ln\left(\frac{0.038 g M_{\text{Pl}} M_- \langle\sigma v\rangle(x_f)}{(g_* x_f)^{1/2}}\right). \quad (15)$$

Here g represents the number of degrees of freedom of the dark matter particle N_- .

As seen from the left panel of Fig. 2, the relic density with s -channel contribution is featured to meet the Planck limit [62] near the resonance in propagator (H_1, H_2, Z'), i.e., near $M_- = \frac{M_{\text{prop}}}{2}$. We restrict our discussion to the mass region (in GeV), $100 \leq M_{Z'} \leq 1000$, $80 \leq M_- \leq 1000$ and also H_2 is considered to be sufficiently large such that its resonance doesn't meet the Planck limit below 1 TeV region of DM mass. Now, in this mass range of DM, the channels mediated by (Z', η, S_1) drive the relic density observable, where the gauge coupling $g_{\mu\tau}$ controls the s -channel contribution, while $Y_{\beta l}, y_{qR}$ are relevant in t -channel contributions. Hence, the relevant parameters in our investigation are $(M_-, g_{\mu\tau}, M_{Z'}, Y_{\beta l}, y_{qR})$. The effect of these parameters on the relic abundance is made transparent in Fig. 2, where we have considered $Y_{\beta l} \sim 10^{-2}$, in order to explain neutrino mass at one loop level. Left panel shows the variation of relic density with varying gauge parameters $g_{\mu\tau}$ and $M_{Z'}$, right

panel depicts the behavior with varying y_{qR} parameter. No significant constraint on $M_{Z'}$, $g_{\mu\tau}$ parameters is observed, however relic density has an appreciable footprint on $M_- - (y_{qR})^2$ parameter space, which will be discussed in the next section.

B. Direct searches

Moving to direct searches, the Z' mediated WIMP-nucleon interaction is not possible at tree-level as the Z' boson does not couple to quarks. The t -channel scalar (H_1, H_2) exchange can give spin-independent (SI) contribution, but it doesn't help our purpose of study. In the scalar portal, one can obtain contribution from spin-dependent (SD) interaction mediated by SLQ, of the form

$$\mathcal{L}_{\text{eff}}^{\text{SD}} \simeq \frac{y_{qR}^2 \cos^2 \alpha}{4(M_{S_1}^2 - M_-^2)} \overline{N_-} \gamma^\mu \gamma^5 N_- \bar{q} \gamma_\mu \gamma^5 q. \quad (16)$$

The s-channel process is depicted in the left most panel of Fig. 3 and the corresponding cross section is given by [63]

$$\sigma_{\text{SD}} = \frac{\mu_r^2}{\pi} \frac{\cos^4 \alpha}{(M_{S_1}^2 - M_-^2)^2} [y_{dR}^2 \Delta_d + y_{sR}^2 \Delta_s]^2 J_n(J_n + 1), \quad (17)$$

where the angular momentum $J_n = \frac{1}{2}$, reduced mass $\mu_r = \frac{M_- M_n}{M_- + M_n}$ with $M_n \simeq 1$ GeV for nucleon. The values of quark spin functions Δ_q are provided in [63]. Now, it is obvious that it can constrain the parameters M_- and $(y_{qR})^2$. Fig. 4, left panel displays $M_- - (y_{qR})^2$ parameter space (green and red regions) remained after imposing Planck [62] 3σ limit on current relic density. Here, the region shown in green turns out to be excluded by most stringent PICO-60 [64] limit on SD WIMP-proton cross section, as seen from the right panel. Apart from tree-level, one-loop penguin diagrams (middle and right panels of Fig. 3) involving SLQ, mediated by SM neutral gauge boson (Z) and the neutral scalars (H_1, H_2) can provide SD and SI contributions respectively. The effective interaction Lagrangian relevant for SD cross section is given by [66, 67]

$$\mathcal{L}_{\text{eff}}^{\text{SD-loop}} \simeq \xi_{q'} \overline{N_-} \gamma^\mu \gamma^5 N_- \bar{q}' \gamma_\mu \gamma^5 q', \quad (18)$$

where

$$\xi_{q'} = \sum_{q=d,s,b} \frac{y_{qR}^2 \cos^2 \alpha a_{q'}}{32\pi^2 M_Z^2} \left[(v_q + a_q) G \left(\frac{M_-^2}{M_{S_1}^2} \right) \right]. \quad (19)$$

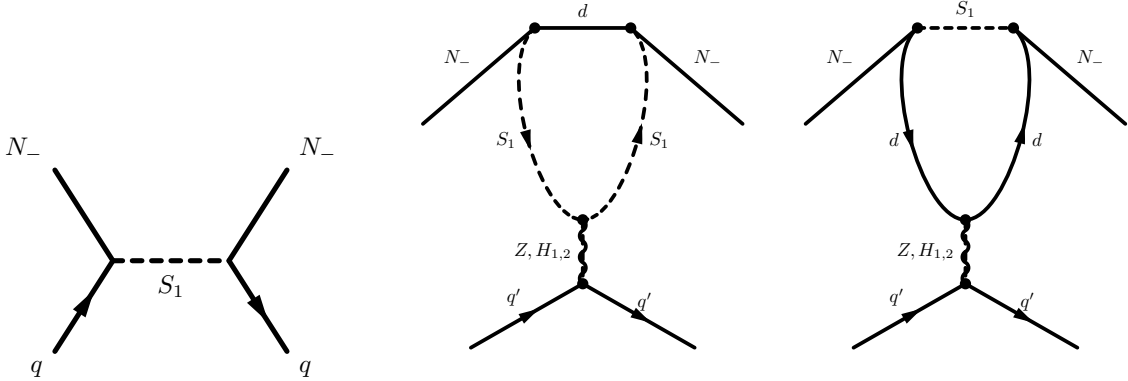


FIG. 3: Diagrams involving SLQ relevant in direct detection study.

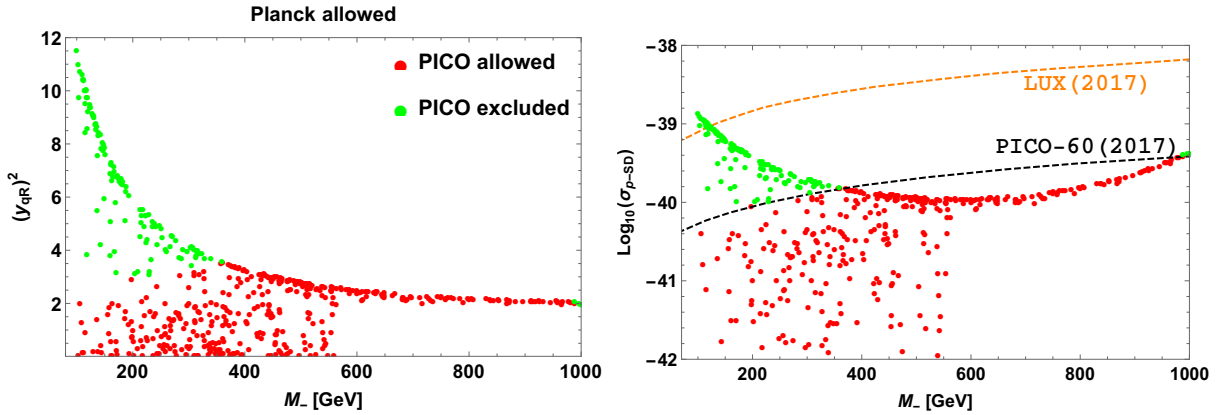


FIG. 4: Left panel depicts the $M_- - (y_{qR})^2$ parameter space consistent upto 3σ level of Planck limit [62] on relic density. Right panel gives the SD WIMP-proton cross section as a function of DM mass. Dashed lines represent the recent bounds obtained from PICO-60 [64] and LUX [65]. Green (red) data points in both the panels represent Planck allowed and PICO excluded (Planck and PICO allowed).

And the loop function takes the form

$$G(x) = -1 + \frac{2(x + (1-x)\ln(1-x))}{x^2}. \quad (20)$$

The corresponding WIMP-nucleon cross section is given by

$$\sigma_{\text{SD}}^{\text{loop}} = \frac{16\mu_r^2}{\pi} J_n(J_n + 1)(\xi_u\Delta_u + \xi_d\Delta_d + \xi_s\Delta_s)^2. \quad (21)$$

In the above expression, $v_q = \frac{g}{2 \cos \theta_w} \left(-\frac{1}{2} + \frac{2}{3} \sin^2 \theta_w \right)$, $a_q = -\frac{g}{4 \cos \theta_w}$ and $a_{q'} = \frac{g}{4 \cos \theta_w} \left(-\frac{g}{4 \cos \theta_w} \right)$ for $q' = u (d, s)$. For SI contribution, the effective interaction term is

$$\mathcal{L}_{\text{eff}}^{\text{SI-loop}} \simeq \Lambda_{q'} \bar{N}_- N_- \bar{q}' q' . \quad (22)$$

and the corresponding cross-section are given by

$$\sigma_{\text{SI}}^{\text{loop}} = \frac{4\mu_r^2}{\pi} M_n^2 \left(\frac{\Lambda_{q'}}{m_{q'}} \right)^2 f_n^2 , \quad (23)$$

where

$$\Lambda_{q'} = - \sum_{q=d,s,b} \frac{y_{qR}^2 \cos^2 \alpha}{16\pi^2} \left[\frac{\lambda_{HS} v \cos \zeta - \lambda_{S2} v_2 \sin \zeta}{M_{H_1}^2} + \frac{\lambda_{HS} v \sin \zeta + \lambda_{S2} v_2 \cos \zeta}{M_{H_2}^2} \right] G_1 \left(\frac{M_-^2}{M_{S_1}^2} \right) \frac{m_{q'}}{v M_-} .$$

Here $G_1(x) = \frac{x + (1-x)\ln(1-x)}{x}$. For proton, the typical value of the scalar form factor f_n is ~ 0.3 . Fig. 5, left and right panels project the one-loop SD and SI contributions respectively for the parameter space consistent with Planck data. We see that these contributions are well below the current upper limits set by direct detection collaborations such as PICO-60 [64], LUX [65] for SD and PandaX-II [68], XENON1T [69], LUX [70] for SI cases. Thus they do not have any impact on the range of model parameters.

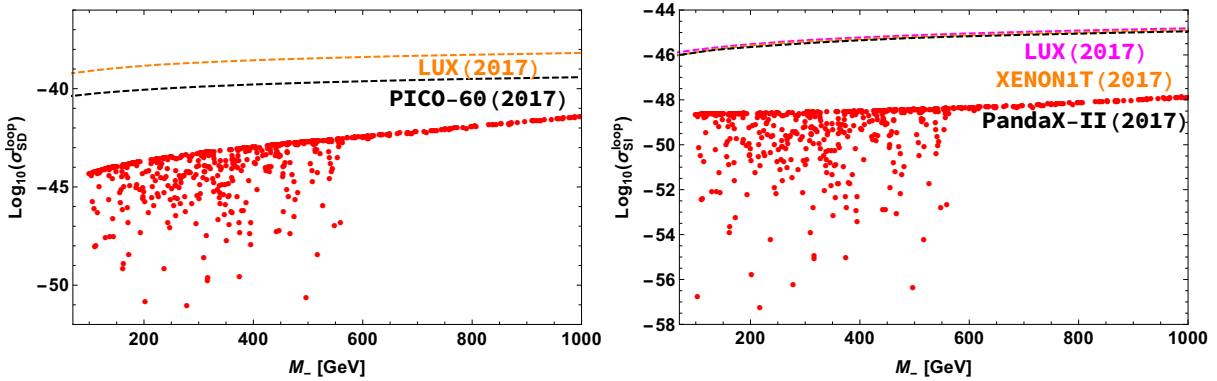


FIG. 5: One-loop SD and SI contributions projected in the left and right panels respectively. Stringent upper limits of PICO-60 [64] and LUX [65] are given in the left panel, PandaX-II [68], XENON1T [69] and LUX [70] bounds are provided in the right panel.

V. RADIATIVE NEUTRINO MASS

The light neutrino mass can be generated at one-loop level from the Yukawa interaction with inert doublet in Eqn. 5. and the corresponding diagram is shown in Fig. 6. Assuming $m_0^2 = (M_{\eta_e}^2 + M_{\eta_o}^2)/2$ is much greater than $M_{\eta_e}^2 - M_{\eta_o}^2 = \lambda''_{H\eta} v^2$, the expression for the radiatively generated neutrino mass [71] is given by

$$(\mathcal{M}_\nu)_{\beta\gamma} = \frac{\lambda''_{H\eta} v^2}{16\pi^2} \sum_{l=e,\mu,\tau} \frac{Y_{\beta l} Y_{\gamma l} M_{Dl}}{m_0^2 - M_{Dl}^2} \left[1 + \frac{M_{Dl}^2}{m_0^2 - M_{Dl}^2} \ln \frac{M_{Dl}^2}{m_0^2} \right]. \quad (24)$$

Here $M_{Dl} = (U^T M_N U)_l = \text{diag}(M_{ee}, M_-, M_+)$ and the fermion mass eigenstates $N_{Dl} = U_{lm}^\dagger N_m$. The light neutrino mass matrix (24) can be expressed as

$$(\mathcal{M}_\nu)_{\beta\gamma} \equiv (Y^T \Lambda Y)_{\beta\gamma}, \quad (25)$$

where the matrix Λ is defined as $\Lambda = \text{diag}(\Lambda_1, \Lambda_2, \Lambda_3)$, with

$$\Lambda_l = \frac{\lambda''_{H\eta} v^2}{16\pi^2} \frac{M_{Dl}}{m_0^2 - M_{Dl}^2} \left[1 + \frac{M_{Dl}^2}{m_0^2 - M_{Dl}^2} \ln \frac{M_{Dl}^2}{m_0^2} \right]. \quad (26)$$

Generation-wise, the $L_\mu - L_\tau$ charges of SM leptons match with the charges of new fermions N_l (0, +1, -1 respectively). The Yukawa interaction term is written using an inert doublet η with vanishing $L_\mu - L_\tau$ charge, and thus the Yukawa matrix $Y_{\beta l}$ takes diagonal form. Hence, the neutrino mass matrix (25) is diagonal, by model construction i.e., $\mathcal{M}_\nu = \text{diag}(M_1, M_2, M_3)$. In order to find the viable region for model parameters consistent with the current neutrino oscillation data, i.e., $6.93 \leq \Delta M_{\text{sol}}^2 [10^{-5} \text{ eV}^2] \leq 7.97$, $2.37 \leq \Delta M_{\text{atm}}^2 [10^{-3} \text{ eV}^2] \leq 2.63$ [72], and cosmological bound on the sum of the light neutrino mass, $\sum_i M_i < 0.23 \text{ eV}$ [73], we perform a scan by varying the parameters in the following range (where the masses are considered in GeV):

$$\begin{aligned} 1000 \leq M_{ee} \leq 3000, \quad 100 \leq M_- \leq 1000, \quad 2000 \leq M_+ \leq 5000, \quad 1000 \leq m_0 \leq 2000, \\ 0.0001 \leq Y_{ee}, Y_{\mu\mu}, Y_{\tau\tau} \leq 0.05. \end{aligned} \quad (27)$$

The allowed parameter space in $Y_{ll} - M_-$ plane, satisfying the above constraints from the neutrino sector is shown in Figure 7. Thus, the proposed model gives viable region of parameter space consistent with recent oscillation data in the context of radiative light neutrino mass matrix.

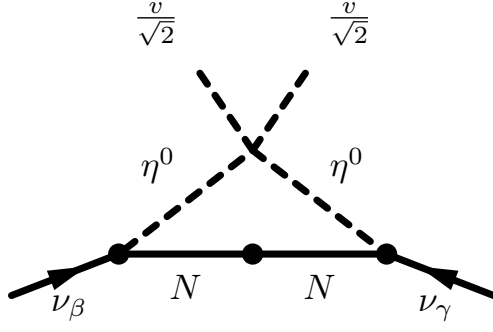


FIG. 6: Radiative generation of neutrino mass.

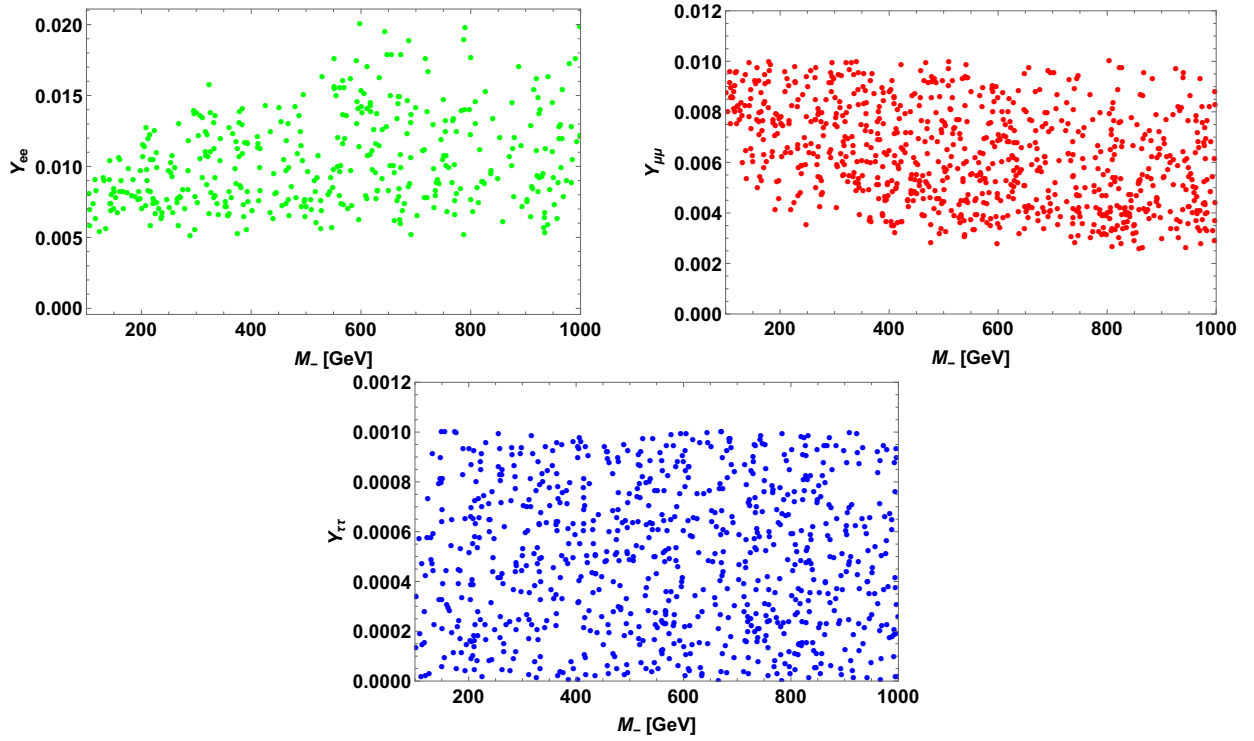


FIG. 7: Allowed parameter space consistent with the current data from neutrino sector in $Y_l - M_-$ plane.

VI. FLAVOR PHENOMENOLOGY

The general effective Hamiltonian responsible for the quark level transition $b \rightarrow sl^+l^-$ is given by [74, 75]

$$\mathcal{H}_{\text{eff}} = -\frac{4G_F}{\sqrt{2}}V_{tb}V_{ts}^* \left[\sum_{i=1}^6 C_i(\mu)O_i + \sum_{i=7,9,10} \left(C_i(\mu)O_i + C'_i(\mu)O'_i \right) \right], \quad (28)$$

where G_F is the Fermi constant and $V_{qq'}$ denote the Cabibbo-Kobayashi-Maskawa (CKM) matrix elements. The C_i 's stand for the Wilson coefficients evaluated at the renormalized scale $\mu = m_b$ [76], where the sum over i includes the current-current operators ($i = 1, 2$) and the QCD-penguin operators ($i = 3, 4, 5, 6$). The quark level operators mediating leptonic/semileptonic processes are given as

$$\begin{aligned} O_7^{(\prime)} &= \frac{e}{16\pi^2} \left[\bar{s} \sigma_{\mu\nu} (m_s P_{L(R)} + m_b P_{R(L)}) b \right] F^{\mu\nu}, \\ O_9^{(\prime)} &= \frac{\alpha_{\text{em}}}{4\pi} (\bar{s} \gamma^\mu P_{L(R)} b) (\bar{l} \gamma_\mu l), \quad O_{10}^{(\prime)} = \frac{\alpha_{\text{em}}}{4\pi} (\bar{s} \gamma^\mu P_{L(R)} b) (\bar{l} \gamma_\mu \gamma_5 l), \end{aligned} \quad (29)$$

where α_{em} denotes the fine-structure constant and $P_{L,R} = (1 \mp \gamma_5)/2$ are the chiral operators. The primed operators are absent in the SM, but can exist in the proposed $L_\mu - L_\tau$ model.

The previous section has discussed the available new parameter space consistent with the DM observables which are within their respective experimental limits. However, these parameters can be further constrained from the quark and lepton sectors, to be presented in the subsequent sections.

A. $B_s - \bar{B}_s$ mixing

In this subsection, we discuss the constraint on the new parameters from the mass difference between the B_s meson mass eigenstates (ΔM_s), which characterizes the $B_s - \bar{B}_s$ mixing phenomena. In the SM, $B_s - \bar{B}_s$ mixing proceeds to an excellent approximation through the box diagram with internal top quark and W boson exchange. The effective Hamiltonian describing the $\Delta B = 2$ transition is given by [77]

$$\mathcal{H}_{\text{eff}} = \frac{G_F^2}{16\pi^2} \lambda_t^2 M_W^2 S_0(x_t) \eta_B (\bar{s}b)_{V-A} (\bar{s}b)_{V-A}, \quad (30)$$

where $\lambda_t = V_{tb}V_{ts}^*$, η_B is the QCD correction factor and the loop function $S_0(x_t)$ is given by [77]

$$S_0(x_t) = \frac{4x_t - 11x_t^2 + x_t^3}{4(1-x_t)^2} - \frac{3}{2} \frac{\log x_t x_t^3}{(1-x_t)^3}, \quad (31)$$

with $x_t = m_t^2/M_W^2$. Using Eqn. (30), the $B_s - \bar{B}_s$ mass difference in the SM is given as

$$\Delta M_s^{\text{SM}} = 2|M_{12}^{\text{SM}}| = \frac{\langle \bar{B}_s | \mathcal{H}_{\text{eff}} | B_s \rangle}{M_{B_s}} = \frac{G_F^2}{6\pi^2} M_W^2 \lambda_t^2 \eta_B \hat{B}_s f_{B_s}^2 M_{B_s} S_0(x_t). \quad (32)$$

The SM predicted value of ΔM_s by using the input parameters from [78, 79] is

$$\Delta M_s^{\text{SM}} = (17.426 \pm 1.057) \text{ ps}^{-1}, \quad (33)$$

and the corresponding experimental value is [78]

$$\Delta M_s^{\text{Expt}} = 17.761 \pm 0.022 \text{ ps}^{-1}. \quad (34)$$

Even though the theoretical prediction is in good agreement with the experimental $B_s - \bar{B}_s$ oscillation data, it does not completely rule out the possibility of new physics.

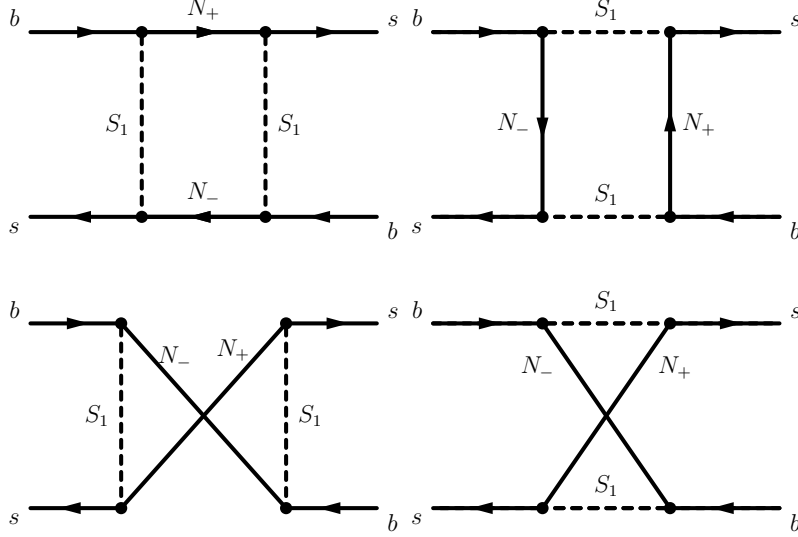


FIG. 8: Box diagrams of $B_s - \bar{B}_s$ mixing with leptoquark in the loop.

The box diagrams for $B_s - \bar{B}_s$ mixing in the presence of singlet SLQ and N_{\pm} are shown in Fig. 8. The effective Hamiltonian in the presence NP is given by

$$\mathcal{H}_{\text{eff}} = \frac{(y_{sR}y_{bR})^2}{128\pi^2 M_{S_1}^2} \cos^2 \alpha \sin^2 \alpha C_{B_s}^{\text{NP}} (\bar{s}b)_{V+A} (\bar{s}b)_{V+A}, \quad (35)$$

where

$$\begin{aligned} C_{B_s}^{\text{NP}} &= 2k(\chi_-, \chi_-, 1) + 4k(\chi_-, \chi_+, 1) + 2k(\chi_+, \chi_+, 1) + \chi_- j(\chi_-, \chi_-, 1) \\ &+ 2\sqrt{\chi_- \chi_+} j(\chi_-, \chi_+, 1) + \chi_+ j(\chi_+, \chi_-, 1), \end{aligned} \quad (36)$$

with $\chi_{\mp} = M_{\mp}^2/M_{S_1}^2$ and the loop functions $k(\chi_{\pm}, \chi_{\mp}, 1)$, $j(\chi_{\pm}, \chi_{\mp}, 1)$ are given in Appendix A. Using Eqn. (35), the mass difference of $B_s - \bar{B}_s$ mixing due to the exchange of S_1 and N_{\pm} is found to be

$$\Delta M_s^{\text{NP}} = \frac{(y_{sR}y_{bR})^2}{48\pi^2 M_{S_1}^2} \cos^2 \alpha \sin^2 \alpha C_{B_s}^{\text{NP}} \eta_B \hat{B}_{B_s} f_{B_s}^2 M_{B_s}. \quad (37)$$

Including the NP contribution arising due to the SLQ exchange, the total mass difference can be written as

$$\Delta M_s = \Delta M_s^{\text{SM}} \left[1 + \frac{C_{B_s}^{\text{NP}} \cos^2 \alpha \sin^2 \alpha}{8G_F^2 V_{tb}^2 V_{ts}^{*2} M_W^2 S_0(x_t)} \left(\frac{(y_{sR} y_{bR})^2}{M_{S_1}^2} \right) \right]. \quad (38)$$

Using Eqns. (33) and (34) in (38), one can put bound on $(y_{qR})^2$ and M_- parameters.

B. $B \rightarrow Kl^+l^-$ process

The rare semileptonic $B \rightarrow Kl^+l^-$ process is mediated via $b \rightarrow sl^+l^-$ quark level transitions. In the current framework, the $b \rightarrow sl^+l^-$ transitions can occur via the Z' exchanging one-loop penguin diagrams shown in Fig. 9. The penguin diagram in the left panel is sup-

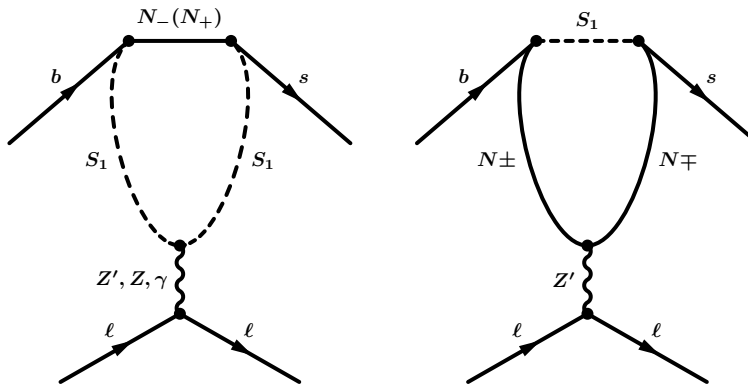


FIG. 9: Penguin diagram of $b \rightarrow sll$ processes, where $l = \mu, \tau$ with leptoquark in the loop.

pressed by the factor, m_b/M_\pm , thus providing negligible contribution. Furthermore, due to the zero hypercharge of dark matter fermion, the diagrams with SM neutral bosons (Z, γ) replacing Z' in the right panel of Fig. 9 are not possible in the present framework. The matrix elements of the various hadronic currents between the initial B meson and K meson in the final state are related to the form factors $f_{+,0}$ as follows [7, 80]

$$\langle K(p_K) | \bar{s} \gamma^\mu b | B(p_B) \rangle = f_+(q^2) (p_B + p_K)^\mu + [f_0(q^2) - f_+(q^2)] \frac{M_B^2 - M_K^2}{q^2} q^\mu, \quad (39)$$

where p_B (p_K) and M_B (M_K) denote the 4-momenta and mass of the B (K) meson and q^2 is the momentum transfer. By using Eqn. (39), the transition amplitude of $B \rightarrow K\mu^+\mu^-$

process is given by

$$\mathcal{M} = \frac{1}{2^5 \pi^2} \frac{y_{bR} y_{sR} g_{\mu\tau}^2}{M_{Z'}^2} \mathcal{V}_{sb}(\chi_-, \chi_+) [\bar{u}(p_B) \gamma^\mu (1 + \gamma_5) u(p_K)] [\bar{v}(p_2) \gamma_\mu u(p_1)], \quad (40)$$

where p_1 and p_2 are the four momenta of charged leptons and the loop function $\mathcal{V}_{sb}(\chi_-, \chi_+)$ is given in Appendix A [20, 81]. Now comparing this amplitude (40) with the amplitude obtained from the effective Hamiltonian (28), we obtain a new Wilson coefficient associated with the right-handed semileptonic electroweak penguin operator \mathcal{O}'_9 as

$$C_9^{\text{NP}} = \frac{\sqrt{2}}{2^4 \pi G_F \alpha_{\text{em}} V_{tb} V_{ts}^*} \frac{y_{bR} y_{sR} g_{\mu\tau}^2}{M_{Z'}^2} \mathcal{V}_{sb}(\chi_-, \chi_+). \quad (41)$$

The differential branching ratio of $B \rightarrow Kll$ process with respect to q^2 is given by

$$\frac{d\text{Br}}{dq^2} = \tau_B \frac{G_F^2 \alpha_{\text{em}}^2 |V_{tb} V_{ts}^*|^2}{2^8 \pi^5 M_B^3} \sqrt{\lambda(M_B^2, M_K^2, q^2)} \beta_l f_+^2 \left(a_l(q^2) + \frac{c_l(q^2)}{3} \right), \quad (42)$$

where

$$\begin{aligned} a_l(q^2) &= q^2 |F_P|^2 + \frac{\lambda(M_B^2, M_K^2, q^2)}{4} (|F_A|^2 + |F_V|^2) \\ &\quad + 2m_l (M_B^2 - M_K^2 + q^2) \text{Re}(F_P F_A^*) + 4m_l^2 M_B^2 |F_A|^2, \\ c_l(q^2) &= -\frac{\lambda(M_B^2, M_K^2, q^2)}{4} \beta_l^2 (|F_A|^2 + |F_V|^2), \end{aligned} \quad (43)$$

with

$$\begin{aligned} F_V &= \frac{2m_b}{M_B} C_7^{\text{eff}} + C_9^{\text{eff}} + C_9^{\text{NP}}, \quad F_A = C_{10}, \\ F_P &= m_l C_{10} \left[\frac{M_B^2 - M_K^2}{q^2} \left(\frac{f_0(q^2)}{f_+(q^2)} - 1 \right) - 1 \right], \end{aligned} \quad (44)$$

and

$$\lambda(a, b, c) = a^2 + b^2 + c^2 - 2(ab + bc + ca), \quad \beta_l = \sqrt{1 - 4m_l^2/q^2}. \quad (45)$$

For numerical estimation, we have used the lifetime and masses of particles from [78] and the form factors are taken from [82]. The experimental limit on the branching ratios of $\bar{B}^0 \rightarrow \bar{K}^0 \mu^+ \mu^-$ and $B^+ \rightarrow K^+ \tau^+ \tau^-$ processes are [78]

$$\text{Br}(\bar{B}^0 \rightarrow \bar{K}^0 \mu^+ \mu^-) \Big|_{\text{Expt}} = (3.39 \pm 0.34) \times 10^{-7}, \quad (46)$$

$$\text{Br}(B^+ \rightarrow K^+ \tau^+ \tau^-) \Big|_{\text{Expt}} < 2.5 \times 10^{-3}, \quad (47)$$

while their predicted values in the SM are

$$\text{Br}(\bar{B}^0 \rightarrow \bar{K}^0 \mu^+ \mu^-) \Big|_{\text{SM}}^{\text{SM}} = (1.82 \pm 0.15) \times 10^{-7}, \quad (48)$$

$$\text{Br}(B^+ \rightarrow K^+ \tau^+ \tau^-) \Big|_{\text{SM}}^{\text{SM}} = (1.56 \pm 0.125) \times 10^{-7}. \quad (49)$$

Since Z' doesn't couple to electron, the branching ratio of $B \rightarrow Ke^+e^-$ process is considered to be SM like. The decay modes $\bar{B}^0 \rightarrow \bar{K}^0 \mu^+ \mu^-$ and $B^+ \rightarrow K^+ \tau^+ \tau^-$ can put constraint on all the four parameters, i.e., $(y_{qR})^2$, $g_{\mu\tau}$, $M_{Z'}$ and M_- .

C. $B \rightarrow X_s \gamma$ process

The $B \rightarrow X_s \gamma$ process involves $b \rightarrow s \gamma$ quark level transition, the experimental limit on the corresponding branching ratio is given by [83]

$$\text{Br}(B \rightarrow X_s \gamma) \Big|_{E_\gamma > 1.6 \text{ GeV}}^{\text{Expt}} = (3.32 \pm 0.16) \times 10^{-4}. \quad (50)$$

Fig. 10 represents the one loop penguin diagram of $b \rightarrow s \gamma$ process mediated by SLQ and N_\pm .

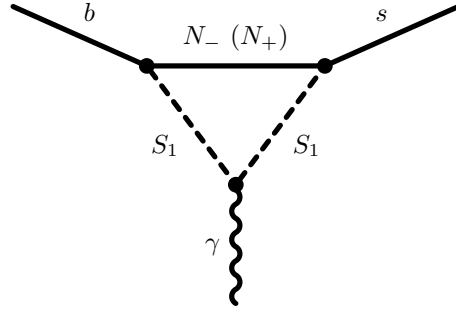


FIG. 10: Feynman diagram of $b \rightarrow s \gamma$ processes in the presence of scalar leptoquark.

Including the NP contribution, the total branching ratio of $B \rightarrow X_s \gamma$ is given by

$$\text{Br}(B \rightarrow X_s \gamma) = \text{Br}(B \rightarrow X_s \gamma) \Big|_{\text{SM}}^{\text{SM}} \left(1 + \frac{C_7^{\gamma \text{NP}}}{C_7^{\gamma \text{SM}}} \right)^2, \quad (51)$$

where the predicted SM branching ratio is [84]

$$\text{Br}(B \rightarrow X_s \gamma) \Big|_{E_\gamma > 1.6 \text{ GeV}}^{\text{SM}} = (3.36 \pm 0.23) \times 10^{-4}. \quad (52)$$

The new $C_7^{\gamma'NP}$ Wilson coefficient obtained from Fig. 10 is given by

$$C_7^{\gamma'NP} = -\frac{\sqrt{2}/3}{8G_F V_{tb} V_{ts}^*} \frac{y_{bR} y_{sR}}{M_{S_1}^2} \left(J_1(\chi_-) \cos^2 \alpha + J_1(\chi_+) \sin^2 \alpha \right), \quad (53)$$

where the loop functions $J_1(\chi_{\pm})$ are given as [20]

$$J_1(\chi_{\pm}) = \frac{1 - 6\chi_{\pm} + 3\chi_{\pm}^2 + 2\chi_{\pm}^3 - 6\chi_{\pm}^2 \log \chi_{\pm}}{12(1 - \chi_{\pm})^4}. \quad (54)$$

Using Eqns. (50, 52, 53) in (51), the parameters $(y_{qR})^2$ and M_- can be constrained.

D. $\tau \rightarrow \mu \nu_{\tau} \bar{\nu}_{\mu}$ process

In the presence of Z' boson, the $\tau \rightarrow \mu \nu_{\tau} \bar{\nu}_{\mu}$ process can occur via box diagram as shown in Fig. 11. There are four possible one-loop box diagrams with the Z' connected to the lepton legs. The total branching ratio of this process is given by [85]

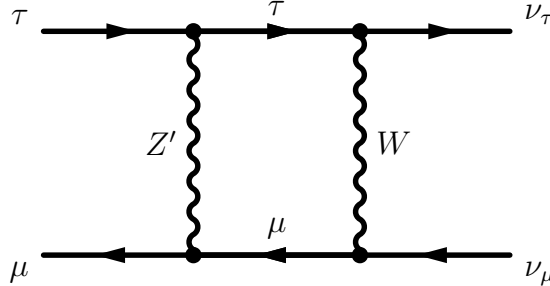


FIG. 11: One loop box diagram of $\tau \rightarrow \mu \nu_{\tau} \bar{\nu}_{\mu}$ processes.

$$\text{Br}(\tau \rightarrow \mu \nu_{\tau} \bar{\nu}_{\mu}) = \text{Br}(\tau \rightarrow \mu \nu_{\tau} \bar{\nu}_{\mu})|^{\text{SM}} \left(1 + \frac{3g_{\mu\tau}^2}{4\pi^2} \frac{\log(M_W^2/M_{Z'}^2)}{1 - M_{Z'}^2/M_W^2} \right)^2, \quad (55)$$

where the branching ratio in the SM is given by [85]

$$\text{Br}(\tau \rightarrow \mu \nu_{\tau} \bar{\nu}_{\mu})|^{\text{SM}} = (17.29 \pm 0.032)\%. \quad (56)$$

Now comparing the theoretical result with the experimental measured value [78]

$$\text{Br}(\tau \rightarrow \mu \nu_{\tau} \bar{\nu}_{\mu})|^{\text{Expt}} = (17.39 \pm 0.04)\%, \quad (57)$$

one can put bounds on $M_{Z'} - g_{\mu\tau}$ parameter space.

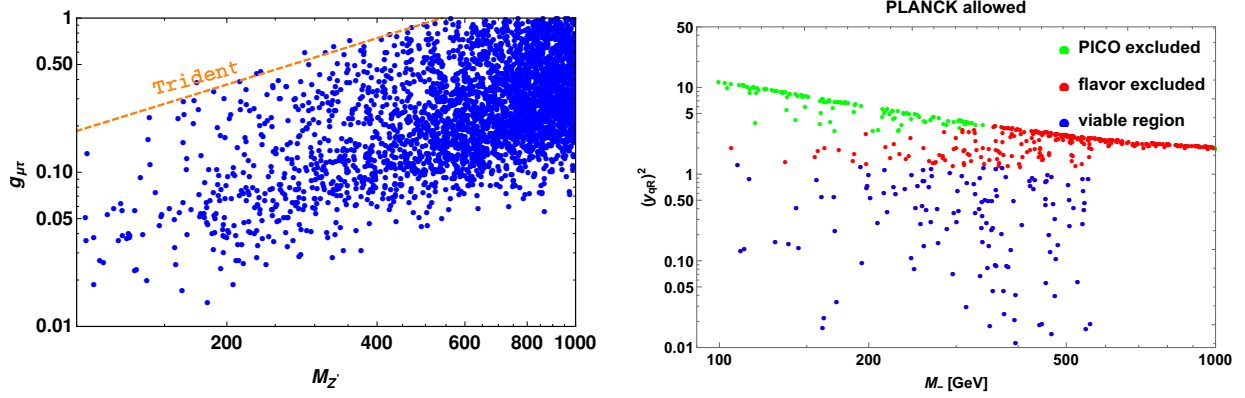


FIG. 12: Left panel projects the constraint on $g_{\mu\tau}$ and $M_{Z'}$ obtained from $\text{Br}(B^+ \rightarrow K^+\tau^+\tau^-)$, $\text{Br}(\bar{B}^0 \rightarrow \bar{K}^0\mu^+\mu^-)$ and $\text{Br}(\tau \rightarrow \mu\nu_\tau\bar{\nu}_\mu)$ observables. Dashed orange line denotes the neutrino trident bound [86, 87]. In the right panel, blue data points denote the allowed parameter space obtained from $\text{Br}(\bar{B}^0 \rightarrow \bar{K}^0\mu^+\mu^-)$, $B_s - \bar{B}_s$ mixing, $\text{Br}(B^+ \rightarrow K^+\tau^+\tau^-)$, $\text{Br}(B \rightarrow X_s\gamma)$ experimental data, which are also consistent with Planck [62] and PICO-60 limit [64]. Here, green (red) data points denote PICO-60 and flavor excluded (PICO-60 allowed and flavor excluded) region.

Parameters	DM-I	DM-II	DM+Flavor
M_- [GeV]	103 – 560	561 – 988	103 – 560
$(y_{qR})^2$	0 – 3.51	1.94 – 2.56	0 – 1.26

TABLE II: Predicted allowed range of parameters M_- and $(y_{qR})^2$. Here DM-I and DM-II represent two regions in Fig. 4 consistent with only DM observables, DM+Flavor denotes the region favored by both the dark matter and flavor studies.

Now correlating the theoretical predictions of $\text{Br}(\bar{B}^0 \rightarrow \bar{K}^0\mu^+\mu^-)$, $\text{Br}(B^+ \rightarrow K^+\tau^+\tau^-)$ and $\text{Br}(\tau \rightarrow \mu\nu_\tau\bar{\nu}_\mu)$ with the corresponding 3σ experimental data, we compute the $M_{Z'} - g_{\mu\tau}$ allowed parameter space. Since Z' does not couple to quarks, these gauge parameters couldn't be constrained from $b \rightarrow s\gamma$ decay modes and $B_s - \bar{B}_s$ oscillation data. The constraint on $M_- - (y_{qR})^2$ parameter space is obtained from $\text{Br}(\bar{B}^0 \rightarrow \bar{K}^0\mu^+\mu^-)$, $\text{Br}(B^+ \rightarrow K^+\tau^+\tau^-)$, $\text{Br}(B \rightarrow X_s\gamma)$ and $B_s - \bar{B}_s$ mixing results. In addition, the branching ratio of rare semileptonic $B \rightarrow K\nu_l\bar{\nu}_l$ process can play a vital role in restricting these parameters. Though the proposed model can allow $b \rightarrow s\nu_l\bar{\nu}_l$ decay modes, but the contributions of μ and τ leptons cancel with each other in the leading order of NP due to their equal and opposite

$L_\mu - L_\tau$ charges. Since there is no $Z'\mu\tau$ coupling, the neutral and charged lepton flavor violating decay processes like $B \rightarrow K^{(*)}\mu^\mp\tau^\pm$, $\tau^- \rightarrow \mu^-\gamma$, $\tau \rightarrow \mu\mu\mu$ do not play any role. It should be noted that, the model considered here provides only additional contribution to $b \rightarrow sll$ transitions through C_9^{NP} coefficient, hence the $B_s \rightarrow l^+l^-$ processes could not provide any strict bound on the new parameters. In this analysis, we consider that the y_{qR} coupling is perturbative, i.e., $|y_{qR}| \lesssim \sqrt{4\pi}$. Left (right) panel in Fig. 12 denotes the parameter space in the plane of $M_{Z'} - g_{\mu\tau}$ ($M_- - (y_{qR})^2$) consistent with DM and flavor studies. From left panel, one can see that the obtained parameter space survives the lower limit imposed on the ratio $M_{Z'}/g_{\mu\tau}$ by neutrino trident production [86, 87], i.e., 540 GeV. It is also noted that the allowed region favored by the $(g-2)_\mu$ anomaly is completely excluded by the constraint from the neutrino trident production [85]. In the right panel of Fig. 12, we redisplay $M_- - (y_{qR})^2$ parameter space of Fig. 4 after a combined analysis made by imposing the DM and flavor experimental limits, with the surviving region shown in blue color. In Table II, we report the allowed region of the parameters M_- and $(y_{qR})^2$ which are consistent with only DM studies (DM-I,II), both DM and flavor sectors (DM+Flavor).

To illustrate the relative contribution of annihilation channels to relic density for the parameter space depicted in Fig. 12, we choose two benchmark values (Table. III), particularly the composition of maximum $(y_{qR})^2$ and minimum $g_{\mu\tau}$ (benchmark-1) and vice-versa (benchmark-2). For these values, we show the relative contribution of each S_1 -portal (Z' -portal) channel in the left (right) panel of Fig. 13. For benchmark-1 i.e., maximal $(y_{qR})^2$, the contribution (blue curve) from SLQ-portal channels - $d\bar{d}, s\bar{s}, b\bar{b}$ ($\sim 32\%$ each) dominate over $(Z', H_{1,2}, \eta)$ -portal contribution (green curve) for almost whole DM mass region except near the resonances in propagators Z', H_1 and H_2 . Similarly, for benchmark-2 i.e., maximal $g_{\mu\tau}$, the Z' -portal channels - $\mu\bar{\mu}, \tau\bar{\tau}, \nu_\mu\bar{\nu}_\mu, \nu_\tau\bar{\nu}_\tau$ ($\sim 24\%$ each) provide dominant contribution (blue curve) over the rest (green curve) with exception to the region near resonances of the propagators H_1 and H_2 . The contribution of the channel with $Z'H_1$ in the final state is negligible due to ζ^2 (Higgs mixing) factor, the process with $Z'H_2$ as final state particles is not kinematically allowed ($M_{H_2} = 2.4$ TeV) for the displayed DM mass range. In the rest of the parameter region of Fig. 12, the dominant contribution however, depends on all the four parameters listed in Table. III.

S.No	$(y_{qR})^2$	$g_{\mu\tau}$	$M_{Z'}$ [GeV]	M_- [GeV]
1.	1.016	0.336	669.84	291.22
2.	0.0003	0.94	763.29	496.7

TABLE III: Sample benchmark values chosen from the allowed parameter space of Fig. 12.

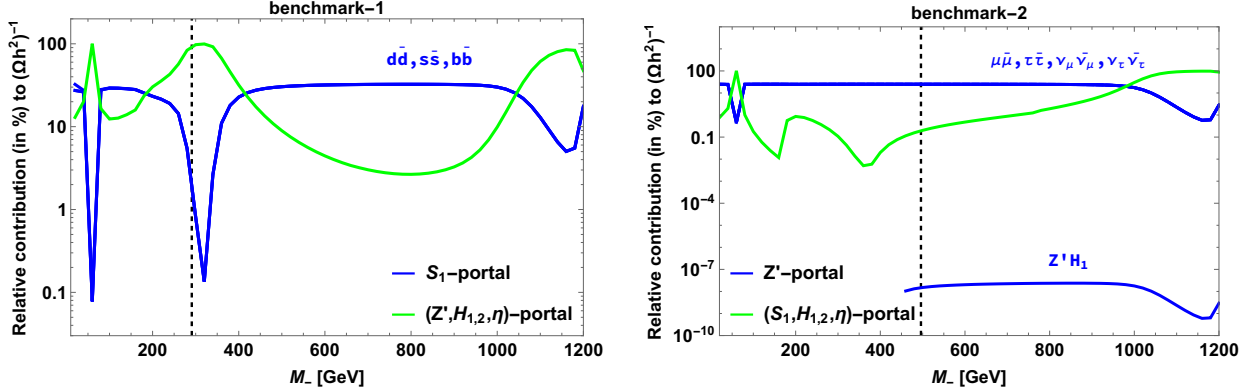


FIG. 13: Left and right panels depict the relative contribution of annihilation channels for the benchmark values of Table. III. Vertical dashed line represents value of DM mass corresponding to the benchmark.

VII. IMPLICATION ON R_K AND $B_{(s)} \rightarrow K^*(\phi)\mu^+\mu^-$ PROCESSES

The constrained parameter space discussed in the previous section can have an impact on R_K and the observables of $B \rightarrow Vl^+l^-$ process, where $V = K^*, \phi$ are the vector mesons, which subsequently decay into $K^* \rightarrow K\pi$ and $\phi \rightarrow K^+K^-$ states. The $B \rightarrow V$ hadronic matrix elements of the local quark bilinear operators can be parametrized as [88, 89]

$$\begin{aligned} \langle V(k) | \bar{s}\gamma_\mu(1 - \gamma_5)b | B(p) \rangle = & \epsilon_{\mu\nu\alpha\beta} \epsilon^{*\nu} p^\alpha q^\beta \frac{2V(q^2)}{M_B + M_V} - i\epsilon_\mu^*(M_B + M_V)A_1(q^2) \\ & + i(\epsilon^* \cdot q)(2p - q)_\mu \frac{A_2(q^2)}{M_B + M_V} + i\frac{2M_V}{q^2}(\epsilon^* \cdot q) [A_3(q^2) - A_0(q^2)] q_\mu, \end{aligned} \quad (58)$$

where

$$A_3(s) = \frac{(M_B + M_V)}{2M_V} A_1(s) - \frac{(M_B - M_V)}{2M_V} A_2(s), \quad (59)$$

q^2 is the momentum transfer between the B and V mesons, i.e., $q_\mu = p_\mu - k_\mu$ and ϵ_μ is the polarization vector of the V meson. The full angular differential decay distribution for the processes $B^0 \rightarrow (K^{*0} \rightarrow K^-\pi^+)l^+l^-$ and $B_s \rightarrow (\phi \rightarrow K^+K^-)l^+l^-$ in terms of q^2 , θ_l , θ_V and

ϕ variables is given as [90–92]

$$\frac{d^4\Gamma}{dq^2 d\cos\theta_l d\cos\theta_V d\phi} = \frac{9}{32\pi} J(q^2, \theta_l, \theta_V, \phi), \quad (60)$$

where

$$\begin{aligned} J(q^2, \theta_l, \theta_V, \phi) = & J_1^s \sin^2 \theta_V + J_1^c \cos^2 \theta_V + (J_2^s \sin^2 \theta_V + J_2^c \cos^2 \theta_V) \cos 2\theta_l \\ & + J_3 \sin^2 \theta_V \sin^2 \theta_l \cos 2\phi + J_4 \sin 2\theta_V \sin 2\theta_l \cos \phi + J_5 \sin 2\theta_V \sin \theta_l \cos \phi \\ & + (J_6^s \sin^2 \theta_V + J_6^c \cos^2 \theta_V) \cos \theta_l + J_7 \sin 2\theta_V \sin \theta_l \sin \phi \\ & + J_8 \sin 2\theta_V \sin 2\theta_l \sin \phi + J_9 \sin^2 \theta_V \sin^2 \theta_l \sin 2\phi, \end{aligned} \quad (61)$$

θ_l is the angle between l^- and $B_{(s)}$ in the dilepton frame, θ_V is defined as the angle between K^- and $B_{(s)}$ in the $K^-\pi^+$ (K^-K^+) frame, the angle between the normal of the $K^-\pi^+$ (K^-K^+) and the dilepton planes is given by ϕ . The complete expressions for $J_i^{s(c)}$, $i = 1, 2, \dots, 9$ as a function of transversity amplitudes are given in the Appendix B [93]. The transversity amplitudes written in terms of the form factors and Wilson coefficients are as follows [93]

$$\begin{aligned} A_{\perp L,R} &= N\sqrt{2\lambda} \left[((C_9^{\text{eff}} + C_9^{\text{NP}}) \mp C_{10}) \frac{V(q^2)}{M_B + M_V} + \frac{2m_b}{q^2} C_7 T_1(q^2) \right], \\ A_{\parallel L,R} &= -N\sqrt{2}(M_B^2 - M_V^2) \left[((C_9^{\text{eff}} - C_9^{\text{NP}}) \mp C_{10}) \frac{A_1(q^2)}{M_B - M_V} + \frac{2m_b}{q^2} C_7 T_2(q^2) \right], \\ A_{0L,R} &= -\frac{N}{2M_V\sqrt{s}} \left[(C_9^{\text{eff}} - C_9^{\text{NP}}) \mp C_{10} \right. \\ &\quad \times \left((M_B^2 - M_V^2 - q^2)(M_B + M_V)A_1(q^2) - \lambda \frac{A_2(q^2)}{M_B + M_V} \right) \\ &\quad \left. + 2m_b C_7 \left((M_B^2 + 3M_V^2 - q^2)T_2(q^2) - \frac{\lambda}{M_B^2 - M_V^2} \right) \right], \\ A_t &= 2N\sqrt{\frac{\lambda}{q^2}} C_{10} A_0(q^2), \end{aligned} \quad (62)$$

where

$$N = V_{tb}V_{ts}^* \left[\frac{G_F^2 \alpha_{\text{em}}^2}{3 \cdot 2^{10} \pi^5 M_B^3} q^2 \beta_l \sqrt{\lambda} \right]^{1/2}, \quad \lambda = \lambda(M_V^2, M_B^2, q^2). \quad (63)$$

The dilepton invariant mass spectrum for $B \rightarrow Vl^+l^-$ decay after integration over all angles [90] is given by

$$\frac{d\Gamma}{dq^2} = \frac{3}{4} \left(J_1 - \frac{J_2}{3} \right), \quad (64)$$

where $J_i = 2J_i^s + J_i^c$. The most interesting observables in these decay modes are the lepton non-universality parameter defined as

$$R_V = \frac{\text{Br}(B \rightarrow V\mu^+\mu^-)}{\text{Br}(B \rightarrow Ve^+e^-)}, \quad (65)$$

and the form factor independent (FFI) observables [94]

$$P'_4 = \frac{J_4}{\sqrt{-J_2^s J_2^c}}, \quad P'_5 = \frac{J_5}{2\sqrt{-J_2^s J_2^c}}. \quad (66)$$

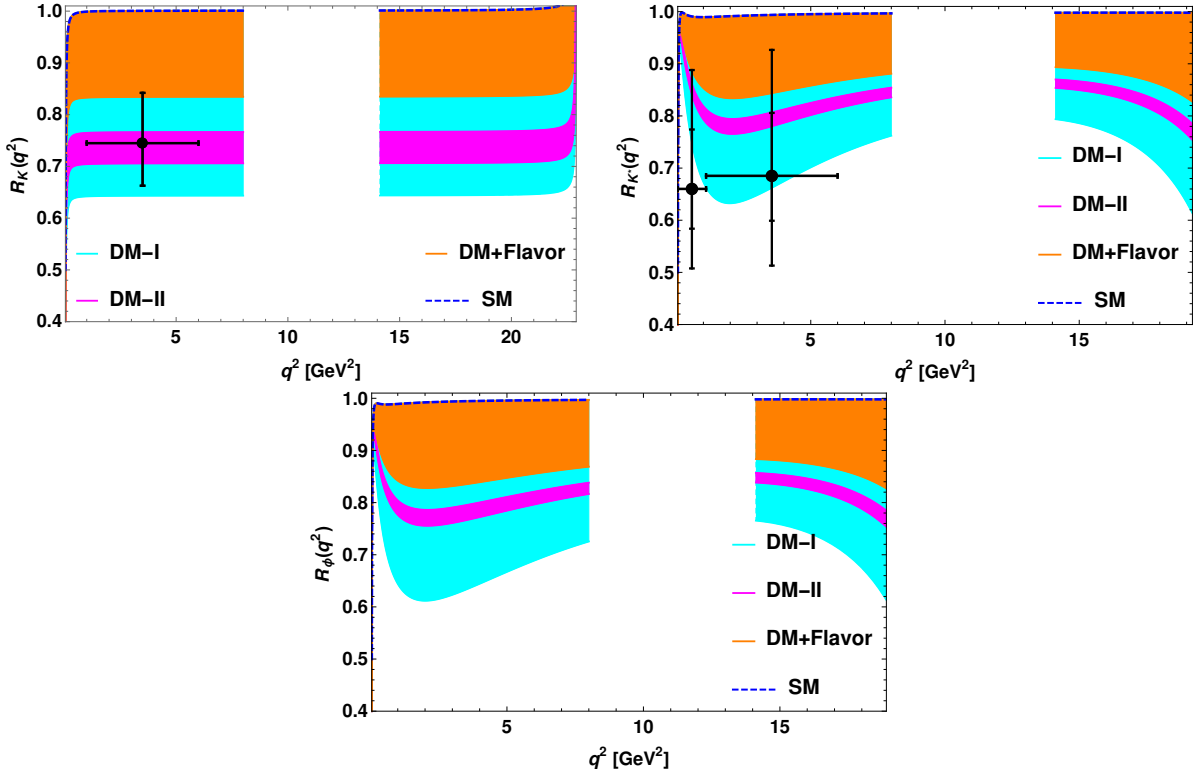


FIG. 14: The q^2 variation of R_K (top-left panel), R_{K^*} (top-right panel) and R_ϕ (bottom panel) LNU parameters in the $L_\mu - L_\tau$ model. Here the blue dashed lines represent the SM prediction, the cyan (magenta) bands stand for the NP contribution from the dark matter studies i.e., DM-I (DM-II). Orange bands are due to the contribution from both the flavor and DM sectors (DM+Flavor). The experimental data points (with 2σ error bars) [1] are shown in black lines .

After getting familiar with the different observables and the allowed values of the new parameters, we now proceed for numerical analysis in the full dilepton mass region i.e., $4m_l^2 \leq q^2 \leq (M_B - M_V)^2$, leaving the regions around $q^2 \sim m_{J/\psi}^2$ and $m_{\psi'}^2$. The cuts are

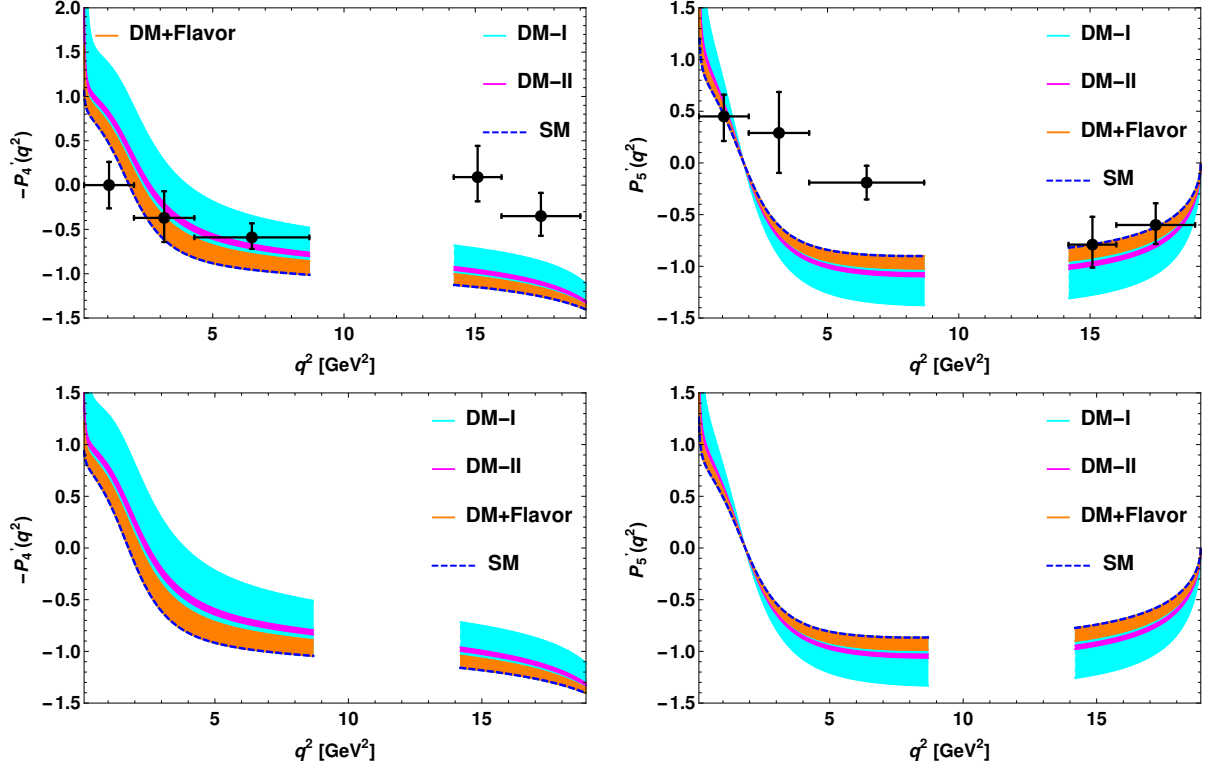


FIG. 15: Top panel represents the variation of P'_4 (left panel) and P'_5 (right panel) observables of $B^0 \rightarrow K^{*0} \mu^+ \mu^-$ process with respect to q^2 . The behaviour of P'_4 (left panel) and P'_5 (right panel) for $B_s \rightarrow \phi \mu^+ \mu^-$ are shown in the bottom panel. The bin-wise experimental data points with error bars are shown in black [4]. Note that $P'_4|_{\text{LHCb}} = -P'_4$.

employed to remove the dominant charmonium resonance $(c\bar{c}) = J/\psi, \psi'$ backgrounds from $B \rightarrow V(c\bar{c}) \rightarrow V l^+ l^-$. In Fig. 14, we show the behaviour of R_K (top-left panel), R_{K^*} (top-right panel) and R_ϕ (bottom panel) with respect to q^2 in the full kinematically accessible physical region. In these figures, the blue dashed lines stand for the SM contribution, the orange bands are due to the allowed region of parameters shown in Table II, favored by both DM and flavor (DM+Flavor) and cyan (magenta) bands for only DM case i.e., DM-I (DM-II). The bin-wise experimental values of $R_{K^{(*)}}$ are shown in black. From the top-left panel of Fig. 14, it can be seen that the result obtained in the $q^2 \in [1, 6]$ GeV² bin, by using the constraint from only DM observable is consistent with the experimental data and can be explained within 1σ for DM+Flavor case. The measured value of R_{K^*} in the $q^2 \in [0.045, 1.1]$ GeV² bin can be accommodated within 1σ (DM-I) and 2σ (DM-II and DM+Flavor), $q^2 \in [1.1, 6]$ GeV² bin result can be described within 1σ (DM-II)

and 2σ (DM+Flavor) and is consistent with experimental data for DM-I case. Though there is no experimental evidence for R_ϕ parameter, the additional NP contribution arising from the allowed parameter space of all cases (DM-I,II and DM+Flavor) provide significant deviation from the SM prediction, implying the presence of lepton universality violation in the $B_s \rightarrow \phi\mu^+\mu^-$ process. In Table IV, we present our predicted values of $R_{K^{(*)}}$ and R_ϕ for different bins. The q^2 variation of famous optimized observables $-P'_4$ (top-left panel) and P'_5 (top-right panel) of $B^0 \rightarrow K^{*0}\mu^+\mu^-$ process are depicted in Fig. 15. The bottom panel of this figure describes analogous plots for $B_s \rightarrow \phi\mu^+\mu^-$ process in both the high and low recoil limit. It should be noted that $P'_4|_{\text{LHCb}} = -P'_4$. In the low q^2 region, our predictions on $-P'_4$ observable of $B^0 \rightarrow K^{*0}\mu^+\mu^-$ process is in very good agreement with the LHCb data. For $B^0 \rightarrow K^{*0}\mu^+\mu^-$ decay mode, the model can accommodate the P'_5 observable within 1σ range of the experimental data, in the high and very low q^2 region. We notice considerable deviation between the results of SM and the presented $L_\mu - L_\tau$ model on the $P'_{4,5}$ observables for $B_s \rightarrow \phi\mu^+\mu^-$ decay modes. The numerical values of all these observables are given in Table IV. We found that our results on the angular observables of $B \rightarrow Vll$ process, obtained from DM-I parameter space are almost consistent with the corresponding measured experimental data.

VIII. SUMMARY AND CONCLUSION

Summarizing the article, we have studied Majorana dark matter in a new version of $U(1)_{L_\mu-L_\tau}$ gauge extension of the standard model. The model is free from triangle gauge anomalies with the inclusion of three neutral fermions with $L_\mu - L_\tau$ charges 0, 1 and -1 . A scalar singlet, charged $+2$ under the new $U(1)$ is added to spontaneously break the $L_\mu - L_\tau$ gauge symmetry, thereby giving masses to the new fermions and the neutral boson Z' associated with gauge extension. In addition, the scalar sector is enriched with an inert doublet and a $(\bar{3}, 1, 1/3)$ scalar leptoquark to obtain the neutrino mass at one-loop level and address the flavor anomalies respectively. All the new fermions, leptoquark and inert doublet are assigned with charge -1 under Z_2 symmetry. Choosing the lightest mass eigenstate of the new fermion spectrum as dark matter, we made a thorough study of Majorana dark matter in relic density and direct detection perspective. The channels contributing to relic density are mediated by the scalar leptoquark, Z' and inert doublet components. As Z' doesn't

	Observables	Values for SM	Values for DM-I	Values for DM-II	Values for DM+Flavor
B^0	$R_{K^*} _{q^2 \in [0.045, 1.1]} \text{ GeV}^2$	0.949	0.793 – 0.949	0.852 – 0.863	0.881 – 0.949
	$R_{K^*} _{q^2 \in [1.1, 6]} \text{ GeV}^2$	0.993	0.671 – 0.993	0.786 – 0.811	0.848 – 0.993
	$R_{K^*} _{q^2 \geq 14.18} \text{ GeV}^2$	0.998	0.754 – 0.998	0.832 – 0.851	0.879 – 0.998
K^{*0}	$P'_5 _{q^2 \in [1, 6]} \text{ GeV}^2$	-0.542 ± 0.044	$-0.82 \rightarrow -0.542$	$-0.655 \rightarrow -0.635$	$-0.612 \rightarrow -0.542$
μ^+	$P'_5 _{q^2 \geq 14.18} \text{ GeV}^2$	-0.695 ± 0.056	$-1.165 \rightarrow -0.695$	$-0.894 \rightarrow -0.86$	$-0.818 \rightarrow -0.695$
μ^-	$P'_4 _{q^2 \in [1, 6]} \text{ GeV}^2$	0.563 ± 0.045	$-0.239 \rightarrow 0.563$	0.195 – 0.257	0.334 → 0.563
	$P'_4 _{q^2 \geq 14.18} \text{ GeV}^2$	1.2 ± 0.096	0.787 – 1.2	1.03 – 1.06	1.098 – 1.2
B_s	$R_\phi _{q^2 \in [0.045, 1.1]} \text{ GeV}^2$	0.9499	0.753 – 0.9499	0.828 – 0.844	0.866 – 0.9499
	$R_\phi _{q^2 \in [1.1, 6]} \text{ GeV}^2$	0.994	0.642 – 0.994	0.77 – 0.8	0.839 – 0.994
	$R_\phi _{q^2 \geq 14.18} \text{ GeV}^2$	0.998	0.731 – 0.998	0.82 – 0.84	0.871 – 0.998
ϕ	$P'_5 _{q^2 \in [1, 6]} \text{ GeV}^2$	-0.511 ± 0.041	$-0.766 \rightarrow -0.551$	$-0.618 \rightarrow -0.599$	$-0.578 \rightarrow -0.511$
μ^+	$P'_5 _{q^2 \geq 14.18} \text{ GeV}^2$	-0.645 ± 0.052	$-1.1 \rightarrow -0.645$	$-0.839 \rightarrow -0.805$	$-0.765 \rightarrow -0.645$
μ^-	$P'_4 _{q^2 \in [1, 6]} \text{ GeV}^2$	0.596 ± 0.048	$-0.202 \rightarrow 0.596$	0.228 – 0.29	0.367 → 0.596
	$P'_4 _{q^2 \geq 14.18} \text{ GeV}^2$	1.233 ± 0.099	0.822 – 1.233	1.059 – 1.092	1.13 – 1.233
	$R_K _{q^2 \in [1, 6]} \text{ GeV}^2$	1.0004	0.643 – 1.0004	0.71 – 0.766	0.834 – 1.0004
	$R_K _{q^2 \geq 14.18} \text{ GeV}^2$	1.002	0.645 – 1.002	0.71 – 0.768	0.836 – 1.002

TABLE IV: Predicted numerical values of LNU parameters (R_V) and $P'_{4,5}$ observables of $B_{(s)} \rightarrow V\mu^+\mu^-$, $V = K^*, \phi$ processes in the high and low recoil limits. The values of R_K parameter are also presented in both low and high q^2 regime

couple to quarks, the Z' -mediated tree level interaction for direct detection is not permitted. Only leptoquark portal channels contribute to spin-dependent WIMP-nucleon cross section. Imposing Planck limit on relic density and well known PICO-60, LUX bounds on spin-dependent cross section, we have constrained the new parameters of the model. We have also computed the spin-dependent and spin-independent contributions of one-loop diagrams involving scalar leptoquark, but found to give zero impact on the model parameters. We have also showed the mechanism of generating light neutrino mass radiatively using the inert doublet. A note on the viable parameter region consistent with neutrino oscillation data is also addressed.

We have further restricted the new parameters from quark and lepton sectors i.e., by comparing the theoretical predictions of $\text{Br}(\tau \rightarrow \mu\nu_\tau\bar{\nu}_\mu)$, $\text{Br}(B \rightarrow X_s\gamma)$, $\text{Br}(B^+ \rightarrow K^+\tau^+\tau^-)$, $\text{Br}(\bar{B}^0 \rightarrow \bar{K}^0\mu^+\mu^-)$ and $B_s - \bar{B}_s$ mixing with their corresponding 3σ experimental data. The neutral and charged lepton flavor violating decay processes are absent due to zero $Z'\tau\mu$ coupling. And also the vanishing $Z'q\bar{q}$ coupling restricts the involvement of Z' in $B_s - \bar{B}_s$ mixing, $b \rightarrow s\gamma$ processes at one-loop level. We have then investigated the implication on $P'_{4,5}$, $R_{K^{(*)}}$ and R_ϕ observables of $B_{(s)} \rightarrow K^{(*)}(\phi)l^+l^-$ decay modes in the full kinematically allowed q^2 region for two cases i.e., dark matter and flavor allowed, only dark matter allowed parameter space. We observed that our model can explain the R_K LNU parameter very well. The R_{K^*} observable obtained from the allowed parameter space consistent with only dark matter is found to be within its 1σ and from both dark matter and flavor is within 2σ experimental limit. In the presence of new physics, the violation of lepton universality is observed in $B_s \rightarrow \phi\mu^+\mu^-$ process, thus, can be probed in LHCb experiment. We noticed that the proposed $L_\mu - L_\tau$ model is also able to explain the LHCb experimental data of the famous optimized $P'_{4,5}$ observables of $B^0 \rightarrow K^{*0}\mu^+\mu^-$ process. We also perceived that the form factor independent observables for $B_s \rightarrow \phi\mu^+\mu^-$ decay modes have sizeable deviation from the standard model. We observed that the parameter region satisfying only dark matter observables for $M_- \leq 560$ GeV have a good impact on the flavor anomalies. To conclude, we have made a comprehensive study of Majorana dark matter, neutrino phenomenology and flavor anomalies in a $U(1)_{L_\mu-L_\tau}$ gauge extended model. This simple framework survives all the current experimental limits on dark matter and flavor observables, can be probed in upcoming high luminosity experiments.

Acknowledgments

SS would like to thank Department of Science and Technology (DST) - Inspire Fellowship division, Govt. of India for the financial support through ID No. IF130927. RM would like to thank Science and Engineering Research Board (SERB), Government of India for financial support through grant Nos. SB/S2/HEP-017/2013 and EMR/2017/001448.

Appendix A: Loop functions

The loop functions required to compute the $b \rightarrow sll$ decays are given by [20, 81]

$$\begin{aligned} \mathcal{V}_{sb}(\chi_-, \chi_+) &= \cos^2 \alpha \sin^2 \alpha (1 + 4\sqrt{\chi_- \chi_+} j(\chi_-, \chi_+) - 2k(\chi_-, \chi_+)) \\ &+ 2 \sin^2 \alpha I(\chi_+) + 2 \cos^2 \alpha I(\chi_-), \end{aligned} \quad (\text{A1})$$

where

$$f(\chi_1, \chi_2, \chi_3, \dots) \equiv \frac{f(\chi_1, \chi_3, \dots) - f(\chi_2, \chi_3, \dots)}{\chi_1 - \chi_2}, \quad f = j, \kappa, \quad (\text{A2})$$

with

$$j(\chi) = \frac{\chi \log \chi}{\chi - 1}, \quad (\text{A3})$$

$$\kappa(\chi) = \frac{\chi^2 \log \chi}{\chi - 1}, \quad (\text{A4})$$

$$I(\chi) = \frac{-3\chi^2 + 4\chi - 1 + 2\chi^2 \log \chi}{8(\chi - 1)^2}. \quad (\text{A5})$$

Eqns. (A2, A3, A4) are used to investigate $B_s - \bar{B}_s$ mixing.

Appendix B: J_i coefficients of $B_{(s)} \rightarrow Vll$ processes

The expressions for the J_i coefficients of $B_{(s)} \rightarrow Vll$ process in terms of transversity amplitudes are given by [91, 93]

$$J_1^s = \frac{(2 + \beta_l^2)}{4} \left[|A_\perp^L|^2 + |A_\parallel^L|^2 + (L \rightarrow R) \right] + \frac{4m_l^2}{q^2} \text{Re} (A_\perp^L A_\perp^{R*} + A_\parallel^L A_\parallel^{R*}), \quad (\text{B1})$$

$$J_1^c = |A_0^L|^2 + |A_0^R|^2 + \frac{4m_l^2}{q^2} \left[|A_t|^2 + 2\text{Re} (A_0^L A_0^{R*}) \right] + \beta_l^2 |A_S|^2, \quad (\text{B2})$$

$$J_2^s = \frac{\beta_l^2}{4} [|A_\perp^L|^2 + |A_\parallel^L|^2 + (L \rightarrow R)], \quad (\text{B3})$$

$$J_2^c = -\beta_l^2 [|A_0^L|^2 + (L \rightarrow R)], \quad (\text{B4})$$

$$J_3 = \frac{1}{2} \beta_l^2 [|A_\perp^L|^2 - |A_\parallel^L|^2 + (L \rightarrow R)], \quad (\text{B5})$$

$$J_4 = \frac{1}{\sqrt{2}} \beta_l^2 [\text{Re} (A_0^L A_\parallel^{L*}) + (L \rightarrow R)], \quad (\text{B6})$$

$$J_5 = \sqrt{2} \beta_l \left[\text{Re} (A_0^L A_\perp^{L*}) - (L \rightarrow R) - \frac{m_l}{\sqrt{q^2}} \text{Re} (A_\parallel^L A_S^* + A_\parallel^R A_S^*) \right], \quad (\text{B7})$$

$$J_6^s = 2\beta_l [\text{Re} (A_\parallel^L A_\perp^{L*}) - (L \rightarrow R)], \quad (\text{B8})$$

$$J_6 = 4\beta_l \frac{m_l}{\sqrt{q^2}} \text{Re} [A_0^L A_S^* + (L \rightarrow R)], \quad (\text{B9})$$

$$J_7 = \sqrt{2}\beta_l \left[\text{Im} (A_0^L A_{\parallel}^{L*}) - (L \rightarrow R) + \frac{m_l}{\sqrt{q^2}} \text{Im} (A_{\perp}^L A_S^* + A_{\perp}^R A_S^*) \right], \quad (\text{B10})$$

$$J_8 = \frac{1}{\sqrt{2}}\beta_l^2 [\text{Im} (A_0^L A_{\perp}^{L*}) + (L \rightarrow R)], \quad (\text{B11})$$

$$J_9 = \beta_l^2 [\text{Im} (A_{\parallel}^{L*} A_{\perp}^L) + (L \rightarrow R)], \quad (\text{B12})$$

where

$$A_i A_j^* = A_i^L(q^2) A_j^{*L}(q^2) + A_i^R(q^2) A_j^{*R}(q^2) \quad (i, j = 0, \parallel, \perp), \quad (\text{B13})$$

in shorthand notation.

-
- [1] R. Aaij et al. (LHCb), JHEP **08**, 055 (2017), 1705.05802.
 - [2] R. Aaij et al. (LHCb), Phys. Rev. Lett. **113**, 151601 (2014), 1406.6482.
 - [3] R. Aaij et al. (LHCb), JHEP **07**, 084 (2013), 1305.2168.
 - [4] R. Aaij et al. (LHCb), Phys. Rev. Lett. **111**, 191801 (2013), 1308.1707.
 - [5] R. Aaij et al. (LHCb), JHEP **06**, 133 (2014), 1403.8044.
 - [6] C. Langenbruch (LHCb), in *Proceedings, 50th Rencontres de Moriond Electroweak Interactions and Unified Theories: La Thuile, Italy, March 14-21, 2015* (2015), pp. 317–324, 1505.04160, URL <http://inspirehep.net/record/1370442/files/arXiv:1505.04160.pdf>.
 - [7] C. Bobeth, G. Hiller, and G. Piranishvili, JHEP **12**, 040 (2007), 0709.4174.
 - [8] B. Capdevila, A. Crivellin, S. Descotes-Genon, J. Matias, and J. Virto, JHEP **01**, 093 (2018), 1704.05340.
 - [9] X. G. He, G. C. Joshi, H. Lew, and R. R. Volkas, Phys. Rev. **D43**, 22 (1991).
 - [10] X.-G. He, G. C. Joshi, H. Lew, and R. R. Volkas, Phys. Rev. **D44**, 2118 (1991).
 - [11] A. Crivellin, G. D’Ambrosio, and J. Heeck, Phys. Rev. Lett. **114**, 151801 (2015), 1501.00993.
 - [12] S. Patra, S. Rao, N. Sahoo, and N. Sahu, Nucl. Phys. **B917**, 317 (2017), 1607.04046.
 - [13] A. Biswas, S. Choubey, and S. Khan, JHEP **09**, 147 (2016), 1608.04194.
 - [14] A. Kamada, K. Kaneta, K. Yanagi, and H.-B. Yu, JHEP **06**, 117 (2018), 1805.00651.
 - [15] M. Bauer, S. Diefenbacher, T. Plehn, M. Russell, and D. A. Camargo (2018), 1805.01904.
 - [16] A. Crivellin, G. D’Ambrosio, and J. Heeck, Phys. Rev. **D91**, 075006 (2015), 1503.03477.

- [17] A. Das, T. Nomura, H. Okada, and S. Roy, Phys. Rev. **D96**, 075001 (2017), 1704.02078.
- [18] A. Das, N. Okada, and D. Raut, Eur. Phys. J. **C78**, 696 (2018), 1711.09896.
- [19] A. Das, N. Okada, and D. Raut, Phys. Rev. **D97**, 115023 (2018), 1710.03377.
- [20] S. Baek, Phys. Lett. **B781**, 376 (2018), 1707.04573.
- [21] R. Mandal (2018), 1808.07844.
- [22] G. Arcadi, M. Dutra, P. Ghosh, M. Lindner, Y. Mambrini, M. Pierre, S. Profumo, and F. S. Queiroz (2017), 1703.07364.
- [23] R. Allahverdi, P. S. B. Dev, and B. Dutta, Phys. Lett. **B779**, 262 (2018), 1712.02713.
- [24] H. Georgi and S. L. Glashow, Phys. Rev. Lett. **32**, 438 (1974).
- [25] H. Georgi, AIP Conf. Proc. **23**, 575 (1975).
- [26] P. Langacker, Phys. Rept. **72**, 185 (1981).
- [27] H. Fritzsch and P. Minkowski, Annals Phys. **93**, 193 (1975).
- [28] J. C. Pati and A. Salam, Phys. Rev. **D10**, 275 (1974), [Erratum: Phys. Rev.D11,703(1975)].
- [29] J. C. Pati and A. Salam, Phys. Rev. **D8**, 1240 (1973).
- [30] J. C. Pati and A. Salam, Phys. Rev. Lett. **31**, 661 (1973).
- [31] O. U. Shanker, Nucl. Phys. **B206**, 253 (1982).
- [32] O. U. Shanker, Nucl. Phys. **B204**, 375 (1982).
- [33] B. Schrempp and F. Schrempp, Phys. Lett. **153B**, 101 (1985).
- [34] B. Gripaios, JHEP **02**, 045 (2010), 0910.1789.
- [35] D. B. Kaplan, Nucl. Phys. **B365**, 259 (1991).
- [36] A. K. Alok, B. Bhattacharya, A. Datta, D. Kumar, J. Kumar, and D. London, Phys. Rev. **D96**, 095009 (2017), 1704.07397.
- [37] D. Beirevi and O. Sumensari, JHEP **08**, 104 (2017), 1704.05835.
- [38] G. Hiller and I. Nisandzic, Phys. Rev. **D96**, 035003 (2017), 1704.05444.
- [39] G. D'Amico, M. Nardecchia, P. Panci, F. Sannino, A. Strumia, R. Torre, and A. Urbano, JHEP **09**, 010 (2017), 1704.05438.
- [40] D. Beirevi, S. Fajfer, N. Konik, and O. Sumensari, Phys. Rev. **D94**, 115021 (2016), 1608.08501.
- [41] M. Bauer and M. Neubert, Phys. Rev. Lett. **116**, 141802 (2016), 1511.01900.
- [42] X.-Q. Li, Y.-D. Yang, and X. Zhang, JHEP **08**, 054 (2016), 1605.09308.
- [43] L. Calibbi, A. Crivellin, and T. Ota, Phys. Rev. Lett. **115**, 181801 (2015), 1506.02661.
- [44] M. Freytsis, Z. Ligeti, and J. T. Ruderman, Phys. Rev. **D92**, 054018 (2015), 1506.08896.

- [45] B. Dumont, K. Nishiwaki, and R. Watanabe, Phys. Rev. **D94**, 034001 (2016), 1603.05248.
- [46] I. Dorner, S. Fajfer, A. Greljo, J. F. Kamenik, and N. Konik, Phys. Rept. **641**, 1 (2016), 1603.04993.
- [47] I. de Medeiros Varzielas and G. Hiller, JHEP **06**, 072 (2015), 1503.01084.
- [48] I. Dorsner, J. Drobnak, S. Fajfer, J. F. Kamenik, and N. Kosnik, JHEP **11**, 002 (2011), 1107.5393.
- [49] S. Davidson, D. C. Bailey, and B. A. Campbell, Z. Phys. **C61**, 613 (1994), hep-ph/9309310.
- [50] J. P. Saha, B. Misra, and A. Kundu, Phys. Rev. **D81**, 095011 (2010), 1003.1384.
- [51] R. Mohanta, Phys. Rev. **D89**, 014020 (2014), 1310.0713.
- [52] S. Sahoo and R. Mohanta, New J. Phys. **18**, 013032 (2016), 1509.06248.
- [53] S. Sahoo and R. Mohanta, Phys. Rev. **D93**, 114001 (2016), 1512.04657.
- [54] S. Sahoo and R. Mohanta, Phys. Rev. **D93**, 034018 (2016), 1507.02070.
- [55] S. Sahoo and R. Mohanta, Phys. Rev. **D91**, 094019 (2015), 1501.05193.
- [56] N. Kosnik, Phys. Rev. **D86**, 055004 (2012), 1206.2970.
- [57] B. Chauhan, B. Kindra, and A. Narang, Phys. Rev. **D97**, 095007 (2018), 1706.04598.
- [58] D. Beirevi, I. Dorner, S. Fajfer, N. Konik, D. A. Faroughy, and O. Sumensari, Phys. Rev. **D98**, 055003 (2018), 1806.05689.
- [59] A. Angelescu, D. Beirevi, D. A. Faroughy, and O. Sumensari, JHEP **10**, 183 (2018), 1808.08179.
- [60] S. Singirala, R. Mohanta, S. Patra, and S. Rao (2017), 1710.05775.
- [61] D. Nanda and D. Borah, Phys. Rev. **D96**, 115014 (2017), 1709.08417.
- [62] N. Aghanim et al. (Planck) (2018), 1807.06209.
- [63] P. Agrawal, Z. Chacko, C. Kilic, and R. K. Mishra (2010), 1003.1912.
- [64] C. Amole et al. (PICO), Phys. Rev. Lett. **118**, 251301 (2017), 1702.07666.
- [65] D. S. Akerib et al. (LUX), Phys. Rev. Lett. **118**, 251302 (2017), 1705.03380.
- [66] A. Ibarra, C. E. Yaguna, and O. Zapata, Phys. Rev. **D93**, 035012 (2016), 1601.01163.
- [67] J. Herrero-Garcia, E. Molinaro, and M. A. Schmidt, Eur. Phys. J. **C78**, 471 (2018), 1803.05660.
- [68] X. Cui et al. (PandaX-II), Phys. Rev. Lett. **119**, 181302 (2017), 1708.06917.
- [69] E. Aprile et al. (XENON) (2017), 1705.06655.
- [70] D. S. Akerib et al. (LUX), Phys. Rev. Lett. **118**, 021303 (2017), 1608.07648.

- [71] E. Ma, Phys. Rev. **D73**, 077301 (2006), hep-ph/0601225.
- [72] F. Capozzi, E. Lisi, A. Marrone, D. Montanino, and A. Palazzo, Nucl. Phys. **B908**, 218 (2016), 1601.07777.
- [73] P. A. R. Ade et al. (Planck), Astron. Astrophys. **594**, A13 (2016), 1502.01589.
- [74] C. Bobeth, M. Misiak, and J. Urban, Nucl. Phys. **B574**, 291 (2000), hep-ph/9910220.
- [75] C. Bobeth, A. J. Buras, F. Kruger, and J. Urban, Nucl. Phys. **B630**, 87 (2002), hep-ph/0112305.
- [76] W.-S. Hou, M. Kohda, and F. Xu, Phys. Rev. **D90**, 013002 (2014), 1403.7410.
- [77] T. Inami and C. S. Lim, Prog. Theor. Phys. **65**, 297 (1981), [Erratum: Prog. Theor. Phys.65,1772(1981)].
- [78] M. Tanabashi et al. (Particle Data Group), Phys. Rev. **D98**, 030001 (2018).
- [79] J. Charles et al., Phys. Rev. **D91**, 073007 (2015), 1501.05013.
- [80] P. Ball and R. Zwicky, Phys. Rev. **D71**, 014015 (2005), hep-ph/0406232.
- [81] J. Hisano, T. Moroi, K. Tobe, and M. Yamaguchi, Phys. Rev. **D53**, 2442 (1996), hep-ph/9510309.
- [82] P. Colangelo, F. De Fazio, P. Santorelli, and E. Scrimieri, Phys. Lett. **B395**, 339 (1997), hep-ph/9610297.
- [83] Y. Amhis et al. (HFLAV), Eur. Phys. J. **C77**, 895 (2017), 1612.07233.
- [84] M. Misiak et al., Phys. Rev. Lett. **114**, 221801 (2015), 1503.01789.
- [85] W. Altmannshofer, S. Gori, M. Pospelov, and I. Yavin, Phys. Rev. **D89**, 095033 (2014), 1403.1269.
- [86] S. R. Mishra et al. (CCFR), Phys. Rev. Lett. **66**, 3117 (1991).
- [87] W. Altmannshofer, S. Gori, M. Pospelov, and I. Yavin, Phys. Rev. Lett. **113**, 091801 (2014), 1406.2332.
- [88] A. Ali, P. Ball, L. T. Handoko, and G. Hiller, Phys. Rev. **D61**, 074024 (2000), hep-ph/9910221.
- [89] M. Wirbel, B. Stech, and M. Bauer, Z. Phys. **C29**, 637 (1985).
- [90] C. Bobeth, G. Hiller, and G. Piranishvili, JHEP **07**, 106 (2008), 0805.2525.
- [91] U. Egede, T. Hurth, J. Matias, M. Ramon, and W. Reece, JHEP **10**, 056 (2010), 1005.0571.
- [92] U. Egede, T. Hurth, J. Matias, M. Ramon, and W. Reece, JHEP **11**, 032 (2008), 0807.2589.
- [93] W. Altmannshofer, P. Ball, A. Bharucha, A. J. Buras, D. M. Straub, and M. Wick, JHEP **01**, 019 (2009), 0811.1214.

[94] S. Descotes-Genon, J. Matias, M. Ramon, and J. Virto, JHEP **01**, 048 (2013), 1207.2753.